2014

Comparative Analysis of a Transition Region Bright Point with a Blinker and Coronal Bright Point Using Multiple EIS Emission Lines

N B. Orange

H M. Oluseyi

D L. Chesny

M Patel

K Hesterly

See next page for additional authors

Repository Citation

Authors

N B. Orange, H M. Oluseyi, D L. Chesny, M Patel, K Hesterly, L Preuss, C Neira, and Niescja E. Turner

Comparative Analysis of a Transition Region Bright Point with a Blinker and Coronal Bright Point Using Multiple EIS Emission Lines

N. Brice Orange, Hakeem M. Oluseyi, David L. Chesny, Maulik Patel, Katie Hesterly, Lauren Preuss, Chantale Neira, and Niescja E. Turner

© Springer ●●●●

Abstract

Since their discovery twenty year ago, transition region bright points have never been observed spectroscopically. Bright point properties have not been compared with similar transition region and coronal structures. In this work we have investigated three transient quiet Sun brightenings including a transition region bright point (TR BP), a coronal bright point (CBP) and a blinker. We use time-series observations of the extreme ultraviolet emission lines of a wide range of temperature T ($\log T = 5.3 - 6.4$) from the *EUV imaging spectrometer* (EIS) onboard the *Hinode* satellite. We present the EIS temperature maps and Doppler maps, which are compared with magnetograms from the Michelson Doppler Imager (MDI) onboard the SOHO satellite. Doppler velocities of the TR BP and blinker are ≤ 25 km s^{-1}, which is typical of transient TR phenomena. The Dopper velocities of the CBP were found to be ≤ 20 km s^{-1} with exception of those measured at $\log T = 6.2$ where a distinct bi-directional jet is observed. From an EM loci analysis we find evidence of single and double isothermal components in the TR BP and CBP, respectively. TR BP and CBP loci curves are characterized by broad distributions suggesting the existence of unresolved structure. By comparing and contrasting the physical characteristics of the events we find the BP phenomena are an indication of multi-scaled self similarity, given similarities in both their underlying magnetic field configuration and evolution in relation to EUV flux changes. In contrast, the blinker phenomena and the TR BP are sufficiently dissimilar in their observed properties as to constitute different event classes. Our work is an indication that the measurement of similar characteristics across multiple event types holds class-predictive power, and is a significant step towards automated solar atmospheric multi-class classification of unresolved transient EUV sources. Finally, the analysis performed here establishes a connection between solar quiet region CBPs and jets.

Department of Physics & Space Sciences, Florida Institute of Technology, Melbourne, FL 32901

1. Introduction

Compact stochastic brightenings have been observed throughout the solar atmosphere. Events known as bright points (BP) appear to be ubiquitous across all temperature regimes of the solar atmosphere (Kankelborg *et al.*, 1996; Kankelborg, Walker, and Hoover, 1997). First discovered in early rocket flights using grazing-incidence optics (Krieger, Vaiana, and van Speybroeck, 1971), BPs are among the most widespread and abundant forms of solar activity. They have been observed to occur in active regions (*e.g.*, Romano *et al.*, 2012), coronal holes (Habbal, Withbroe, and Dowdy, 1990; Subramanian, Madjarska, and Doyle, 2010; Doschek *et al.*, 2010), regions of quiet Sun (Habbal, Withbroe, and Dowdy, 1990; Abramenko *et al.*, 2010; Sánchez Almeida *et al.*, 2010), and are usually associated with the magnetic network (Golub *et al.*, 1974; Egamberdiev and Iakovkin, 1983; Kankelborg, Walker, and Hoover, 1997). In all cases BPs occur in association with mixed magnetic flux that undergoes cancellation or rearrangement while being dynamically driven by hydrodynamic flows or flux emergence (P.M. Harvey *et al.* 1985; Webb *et al.*, 1993; K.L.Harvey *et al.* 1994; Priest, Parnell, and Martin, 1994; Kankelborg, Walker, and Hoover, 1997), suggesting that the BP phenomena is a consequence of magnetic reconnection. Indeed, BPs have often been described as being tiny solar active regions (Longcope *et al.*, 2001).

The surface densities of BPs appears to increase with decreasing temperature (Zhang, Kundu, and White, 2001; McIntosh and Gurman, 2005), although the exact functional form remains unknown. Nonetheless, even near the highest temperatures where BPs are observed — and hence away from the peak of their population distribution — BPs have been measured to contribute significantly to the solar irradiance. For example, a survey of X-ray BPs (XBPs) using data from *Yohkoh*/SXT, concluded that these hot XBPs covered $\approx 1.4\%$ of the quiet-Sun surface area and contributed $\approx 5\%$ of the quiet-Sun X-ray irradiance (Zhang, Kundu, and White, 2001). Naive extrapolation of the BP population distribution to lower temperatures suggests that BPs should be even more important contributors to solar irradiance at lower temperatures, such as in the upper TR ($5.0 \leq \log\ T < 6.0$).

The first studies of transition region (TR) BPs were presented by Habbal, Dowdy, and Withbroe (1990) and Dowdy (1993), who compared lower TR BPs observed in the emission of C III $\lambda977.02$ ($\log T = 4.8$) to coronal BPs observed in the emission of Mg X $\lambda624.94$ ($\log T = 6.8$). Dowdy (1993) utilized spectroheliograms in the emission of O VI $\lambda1031.91$ ($\log T = 5.4$), Ne VII $\lambda465.22$ ($\log T = 5.7$), and Mg X $\lambda624.94$ ($\log T = 6.8$) to identify BPs at upper TR temperatures. The focus of these early studies was to determine whether the BPs studied existed thermally and magnetically isolated from the large-scale corona. Both studies confirmed this question.

In an effort to better constrain the distribution of BPs across the upper TR, Bruni (2006) performed a measurement of TR BP surface number densities and radiated powers at two TR temperatures and in three heliographic latitude bands. He used large area upper TR spectroheliograms in the emission of N V $\lambda1238.81$ ($\log T = 5.2$) and Ne VIII $\lambda770.41$ ($\log T = 5.8$) obtained by

the *Solar Ultraviolet Measurements of Emitted Radiation* (SUMER; Wilhelm *et al.*, 1995) spectrometer on 7–8 June 1996 near solar minimum. The flux-calibrated SUMER data were searched for compact brightenings above magnetic bipoles. Bruni (2006) found that the BP contribution was $\approx 20\%$ in the quiet Sun and $\approx 15\%$ in a polar coronal hole at $\log T = 5.2$ and $\approx 10\%$ in the quiet-Sun and $\approx 5\%$ in the polar region at $\log T = 5.8$. The surface densities of TR BPs observed in N V was $\approx 1 \times 10^{-3}\,\mathrm{Mm}^{-2}$ and in Ne VIII it was $\approx 5 \times 10^{-4}\,\mathrm{Mm}^{-2}$. These surface densities may be compared with the surface densities of coronal BPs observed in the SOHO *Extreme-Ultraviolet Imaging Telescope* (EIT; Delaboudinière *et al.*, 1995) 171Å filtergram by Longcope *et al.* (2001), which was $1.3 \times 10^{-4}\,\mathrm{Mm}^{-2}$. If confirmed, Bruni's measurements of surface densities and irradiance contributions are consistent with the trend in the BP distribution seen at coronal temperatures. Bruni (2006) noted that his surface density counting errors due to Type I (false-negative) and Type II (false-positive) errors was $\approx 30\%$. The Type II errors were most likely due to contamination by compact, TR transients known as blinkers (Harrison, 1997; Harrison *et al.*, 1999; Brković, Solanki, and Rüedi, 2001; Bewsher, Parnell, and Harrison, 2002; Parnell, Bewsher, and Harrison, ; Doyle, Roussev, and Madjarska, 2004).

Just as coronal BPs have been associated with magnetic flux cancellation associated with both converging magnetic bipoles (Golub, Krieger, and Vaiana, 1976; Webb *et al.*, 1993; Priest, Parnell, and Martin, 1994) and emerging magnetic flux (Strong *et al.*, 1992), upper TR BPs and blinkers may form a similar dichotomy — depending on how one defines a blinker. Recent studies have suggested that the blinker classification is generally plagued by Type II errors and that a range of phenomena have been grouped together under the blinker designation (Harrison *et al.*, 2003). In this paper we are thus restricting the blinker designation to the types of phenomena observed by Doyle, Roussev, and Madjarska (2004) and others, which are density enhancement events generated by reconnection involving cool plasma tied to emerging magnetic flux and hot coronal plasma confined in pre-existing coronal structures. Likewise, we will define TR BPs as being upper TR structures generated in association with colliding and cancelling photospheric magnetic flux elements.

There is much to be learned from a study combining TR BPs, coronal BPs, and blinkers. First, individual TR BPs have never been observed in multiple emission lines nor have their Doppler signatures been measured. The physics of TR BPs may very well be similar to that of coronal BPs as an additional manifestation of multi-scaled self-similarity in the solar atmosphere (Vlahos and Georgoulis, 2004; Raouafi *et al.*, 2010). Coronal BPs display a wealth of enigmatic dynamic behaviors that if found in TR BPs might provide new insights into plasma heating and acceleration. For example, coronal BPs show periodic flashes or flaring for which there is not currently a consensus model (Zhang *et al.*, 2012; Kamio *et al.*, 2011). The larger of the flaring BPs often exhibit eruptive behavior in the form of jets, thus contributing mass to the solar wind (Madjarska *et al.*, 2012). It has been inferred that some fundamental plasma processes (*e.g.*, the efficiency of magnetic reconnection) varies across the TR (Longcope, 1998; Longcope and Kankelborg, 1999; Bruni, 2006). Therefore, observing a similar physical process under different plasma conditions may be

insightful. On the other hand, blinkers, which are energized by the reconnection of emerging and pre-existing flux, and TR BPs, which are energized by reconnection driven by hydrodynamic flows, both occur under the same TR conditions. Comparing these different processes occurring under similar plasma parameters may also yield new insights. Finally, solar physics is rapidly moving to a new operational mode where machine learning based software is replacing humans as data processors, a trend that will only increase into the future. These software tools require a set of defining event "features" to distinguish classes. Blinkers have already proven to be a classification challenge for human operators (Harrison *et al.*, 2003; Subramanian *et al.*, 2012). Obtaining robust probabilistic classifications of compact transients in general will be a major challenge in the coming years. A comparative study may identify distinguishing features that may be useful in this effort.

The purpose of this paper is to perform the first multi-wavelength spectroscopic study of an individual TR BP and also to perform the first comparative study of TR BPs with coronal BPs and blinkers. The next section presents an overview of the observational data used in our study and its processing. Section 3 describes our techniques for identifying the events we study and measuring their morphologies, line fluxes, Doppler velocity maps, and temperature structures. Section 4 presents the measurement results and their implications for each event. The discussion of our results and a brief summary are provided in Section 5.

2. Observations

To investigate the spectroscopic properties of the BPs we study, data were obtained from the *EUV Imaging Spectrometer* (EIS; Culhane *et al.*, 2007) on the *Hinode* satellite. The EIS data was taken from 11:13:11 UT to 23:12:40 UT at ≈ 45 min intervals on 22 January 2008. The data consists of raster scans with a $2''$ slit width using $1''$ steps resulting in a final field-of-view (FOV) of $119.''8 \times 360''$. A total of ten emission lines with coverage from the upper TR ($\log T = 5.4$) to the corona ($\log T = 6.2$) were used. The emitting ions, the wavelengths of the emission lines, the atomic transitions of the emission lines, and their peak formation temperatures are all given in Table 1.

The EIS level-0 data were processed and calibrated via the standard Solar SoftWare (SSW) routine eis_prep.pro. Additional corrections were made for co-alignment between EIS's short wavelength (171–212 Å) and long wavelength (250–290 Å) bands (Young and Gallagher, 2008); instrument and orbital jitter variations (Shimizu *et al.*, 2007); the sinusoidal spectrum drift of the lines on the CCD due to orbital changes (Mariska *et al.*, 2007), and the tilt of the emission lines on the detector. These corrections resulted in an absolute wavelength calibration of ± 4.4 km s^{-1} (Kamio *et al.*, 2010).

To investigate the magnetic structure of the events studied, we obtained closest-time data from the *Michelson Dopper Imager* (MDI; Scherrer *et al.*, 1995) instrument onboard the SOHO satellite. The full disk MDI line-of-sight (LOS) magnetograms possessed a pixel resolution of $1.''98 \times 1.''98$ and were obtained with a 96-min cadence over the roughly 12 h of EIS observations. MDI level-1.8 magnetogram data, which are the definitively calibrated images of the solar

line-of-sight (LOS) photospheric magnetic field, were processed using the SSW routine mdi_prep.pro for the removal of instrument noise. In order to increase the signal-to-noise ratio, three magnetograms were averaged at each time step.

Table 1. List of EIS spectral emission lines used in the present study.

Ion	Wavelength (Å)	Transition	$\log T$ (K)
O IV	279.80	$2s^2\,2p\,{}^2P_{3/2}$ - $2s^2\,3s\,{}^2S_{1/2}$	5.3
O V	192.90	$2s\,2p\,{}^3P_2$ - $2s\,3d\,{}^3D_3$	5.4
Fe VIII	185.21	$3p^6\,3d\,{}^2D_{5/2}$ - $3p^5\,3d^2\,{}^2F_{7/2}$	5.6
Mg VII	278.75	$2s^2\,2p^2\,{}^3P_2$ - $2s\,2p^3\,{}^3S^1$	5.8
Fe X	184.30	$3s^2\,3p^5\,{}^2P_{1/2}$ - $3s^2\,3p^4\,({}^3P)\,3d\,{}^2P_{3/2}$	6.0
Fe XI	180.40	$3s^2\,3p^4\,{}^3P_2$ - $3s^2\,3p3\,({}^4S)\,3d\,{}^3D_3$	6.1
Fe XII	195.12	$3s^2\,3p^3\,{}^4S_{3/2}$ - $3s^2\,3p^2\,({}^3P)\,3d\,{}^4P_{5/2}$	6.2
Si X	257.14	$2s^2\,2p^3\,{}^4S_{3/2}$ - $2s\,2p^4\,{}^4P_{1/2}$	6.2
Si XI	191.26	$2s^2\,2p^2\,{}^3P_2$ - $2s\,2p^3\,{}^3S_1$	6.3
Fe XV	284.16	$3s^2\,{}^1S_0$ - $3s\,3p\,{}^1P_1$	6.4

To co-align the EIS and MDI data, each of the ten EIS raster scans was mapped to solar coordinates by calibrating each scan's raster positions with respect to Stonyhurst heliographic coordinates (Zarro, 2005). The magnetograms were then co-aligned to each EIS observation time by using the SSW routine drot_map, resulting in a final alignment error of $\lesssim 2''$. This co-alignment error was measured by cross-correlating visually bright EUV coronal plasma structures to strong magnetogram regions. Projection effects were not expected to play a significant role in the co-alignment since each of our images were $\lesssim \pm 100''$ to disk center. Moreover, the observation time differences between the EIS scans and MDI magnetograms were $\lesssim 30$ min.

Event selection was carried out via visual inspection of both coronal and TR images to identify compact and high contrast EUV brightenings. These events were then compared to MDI magnetograms. We selected three events. The first two events, which were an upper TR BP and a coronal BP (CBP), were required to exist in association with photospheric magnetic bipoles. The CBP had its peak temperature in the corona while the upper TR BP showed no discernable coronal emission. The third event, a blinker, was required to be associated with emerging photospheric magnetic flux. The upper TR BP and the coronal BP were both selected at 11:13:11 UT in the Mg VII $\lambda 278.393$ Å ($\log T = 5.8$) emission line. Figure 1 shows these events in two emission lines. The blinker was selected at 16:49:18 UT in the O V $\lambda 192.900$ Å ($\log T = 5.4$) emission line. After each event was selected their heliographic solar coordinates were then tracked throughout the EIS observation sequence by accounting for solar rotation (≈ 0.17 arcsec min^{-1}) and instrument pointing (Sarro and Berihuete, 2011).
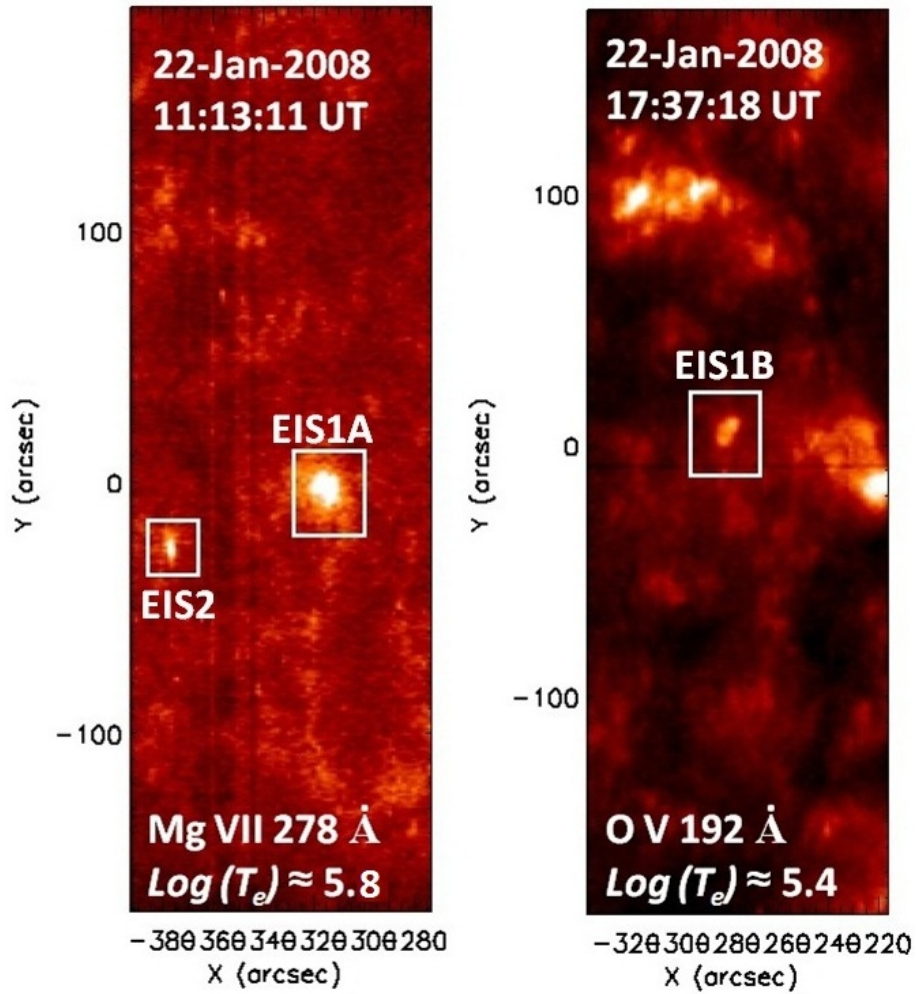
Figure 1. (left) EIS 2″ FFOV intensity image (erg cm^{-2} s^{-1}) in the emission of Mg VII λ278.39 (log $T = 5.8$) observed on 22 January 2008 at 11:13:11 UT. The boxed regions indicate the locations of the EIS1A and EIS2 events. (right) EIS 2″ FOV intensity image (erg cm^{-2} s^{-1}) of O V λ192.90 (log $T = 5.4$) observed on 22 January 2008 at 17:37:18 UT, with boxed regions showing the EIS1B events.

3. Measurements

For each of our three events we have fit the spectrum of each pixel with a Gaussian profile using the SSW routine eis_auto_fit.pro to determine the line intensity at that pixel, the line center at that pixel from which Doppler velocities were derived, and the line width for each pixel from which non-thermal velocities were derived. We note that the O V λ192.90 Å line lies close to the EIS core line Ca XVII λ192.82 Å. Young *et al.* (2007) indicated that Ca XVII is blended with the Fe XI λ192.83 Å line which dominates in most solar conditions. Blending effects in O V were determined to be minimal herein, which is consistent with suggestions
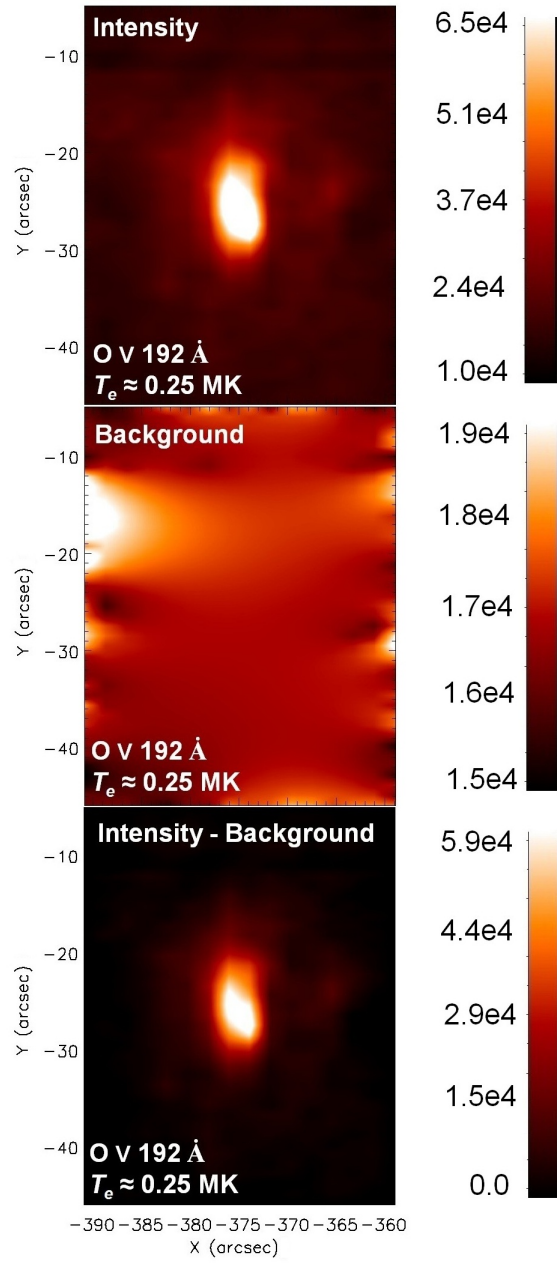
Figure 2. EIS $2''$ intensity (erg cm^{-2} s^{-1} sr^{-1}), background, and intensity minus background images (from top to bottom, respectively) of O v (192.90 Å, $\log T = 5.4$) observed on 22 January 2008 at 11:13:11 UT of the EIS2 event studied here.

that it comprises one half the emission seen at $\lambda192.80\,\text{Å}$ (Young *et al.*, 2007). Event morphology was measured from intensity images. The temperature structure of each event was examined via an emission measure (EM) loci analysis. Magnetic structure of events were determined through direct comparison of MDI line-of-sight magnetograms co-aligned with EUV EIS scans. Details of how each of these measurements were carried out is described in the subsections that follow.

3.1. EUV Intensities and Lifetimes

Measurements of the integrated radiative flux and intensity enhancement of each event was obtained from the EIS intensity maps in each emission line. The first step in our process was to create a model of the background flux in each region of interest (ROI), which was a small rectangular region containing an event in its center with background/foreground emission in the surrounding pixels (Figure 2). This process was necessary since the observed intensity is the superposition of all emission along the line of sight through the optically thin plasma. The background was modeled by first performing a low-pass filter of the ROI in order to remove high-frequency noise such as bad pixels. Next, the border pixels of the ROI — which contained only background/foreground emission — were held constant while the interior of the ROI was boxcar averaged using the standard IDL smoothing procedure. Care was taken to avoid overestimating the background or generating negative pixel values. The result of this procedure was the minimum area surface connecting the border pixels of the ROI. Figure 2 shows an original image of the ROI, an image of the background model, and the background subtracted result. For our events, the background subtraction reduced pixel values by $\lesssim 15\%$.

The integrated flux from each event at each time was calculated in two ways. First, the pixel values of the calibrated and background-subtracted ROIs were summed to obtain the flux F_λ in each line. Second, the 3σ brightest pixels in each line were summed for each event to obtain $F_\lambda^{3\sigma}$. Finally, we calculated intensity enhancement ψ_λ from the data prior to background subtraction using the equation:

$$\psi_\lambda = \frac{F_\lambda^{3\sigma;\text{raw}} - \bar{F}_\lambda^{\text{bg}}}{\bar{F}_\lambda^{\text{bg}}},\qquad(1)$$

where $F_\lambda^{3\sigma;\text{raw}}$ is the average line flux from event pixels in each line λ and $\bar{F}_\lambda^{\text{bg}}$ is the mean solar background emission from each respective image. Uncertainties in ψ_λ were then derived from photon counting statistics in both measurements of F_λ and $\bar{F}_\lambda^{\text{bg}}$.

Upon completing the measurements for all EIS observations we next identified which times the events existed in each line. Times with $\psi_\lambda \geq 10\%$ were flagged as having an existing event. Lifetime measurements require existence continuity for two consecutive time-steps. Events that dropped below this threshold and reemerged later in the time sequence were considered different events given the ≈ 45 min interval between successive EIS observations.
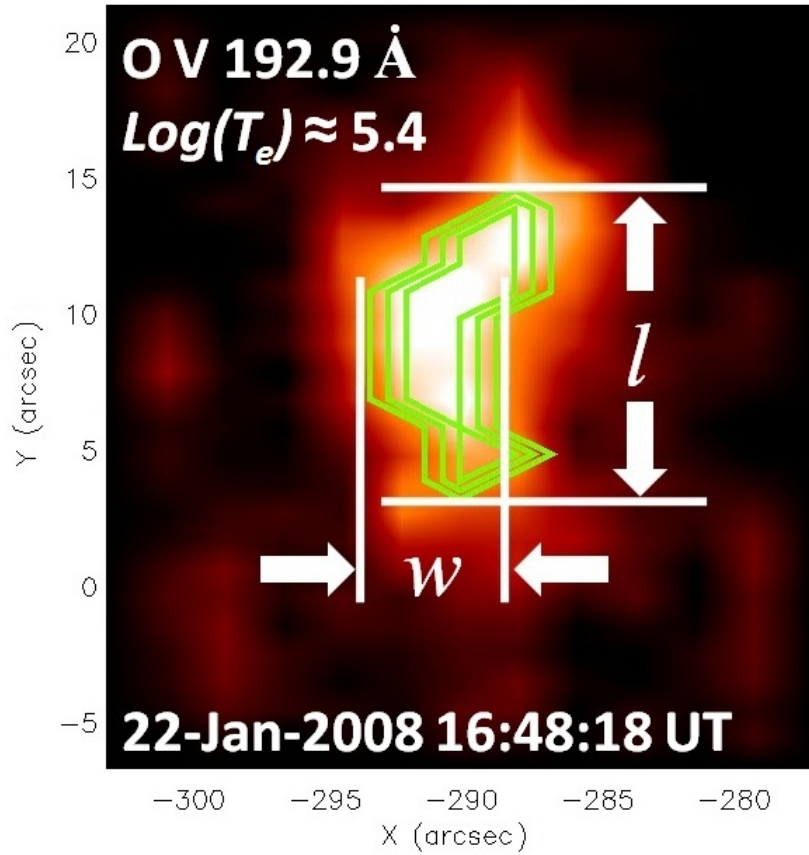
Figure 3. EIS 2″ intensity image (erg cm^{-2} s^{-1} sr^{-1}) of O v λ192.90 (log $T = 5.4$) observed 22 January 2008 at 16:49:18 UT of the EIS1b event. Green contours denote the event-unique pixels derived from our boundary extraction function.

3.2. Morphologies and Doppler Velocities

To measure the morphology of the event, we defined a set of event pixels per isolated thumbnail images. To define these pixel positions, we developed a boundary extraction function comprised of both downhill simplex and clumping techniques to isolate EUV emission enhancements from surrounding solar background. Our boundary extraction function assumes that a given image consists of a single EUV event in which significant contrast and the peak image flux exist. Events' morphologies are measured in each line using the largest spatial widths defined when our boundary extraction function is applied to the image. The greatest extent was labeled l and the greatest width in the direction perpendicular to the greatest extent was labeled w (Figure 3). Radiative areas A_λ (km^2) were then derived from l and w assuming the telescope is at Lagrangian point 1 (≈ 721 km arcsec^{-1}) and propagating uncertainties resultant from 1σ Gaussian fits to the spatial dimensions corresponding to l and w. These quantities were

used with $F_\lambda^{3\sigma}$ to derive luminosities P_λ (erg s^{-1}) of each event as a function of temperature. Luminosity uncertainties were propagated from photon counting statistics and axes length uncertainties.

The event pixels defined by our boundary extraction function were also used to measure, as a function of temperature, the characteristic LOS velocity v_λ (km s^{-1}) for each event by averaging velocities returned by eis_auto_fit.pro and propagating the 1σ fit uncertainties.

3.3. LOS Magnetic Field and Magnetic Flux

For each event, the LOS magnetic field $|B_\ell|$ and flux $|\Phi|$ were measured. We also measured LOS field $|B_\ell|$ and flux $|\Phi|$ of positive and negative polarities. The sizes of the positive and negative polarities $A_B^\pm$ and separation distance d_B were all measured. Note that the separation was not measured for the blinker event that was associated with a single unipolar region.

Signed fluxes were calculated by summing magnetogram pixels of each polarity. The unsigned flux was an integration of the absolute value of both positive or negative polarity fluxes. Magnetic polarity sizes, $A_B^\pm$, were obtained from the number of pixels used calculating signed fluxes. Measurements of separation distance d_B were derived from calculations of the distance between the centroids of the positive and negative magnetic source elements. Uncertainties in LOS magnetic fields were derived from photon counting statistics on individual magnetogram pixels.

3.4. Temperature Structure

To measure the amount of plasma emitting at a particular temperature we began with the standard definition of the column emission measure (EM),

$$\mathrm{EM} = \int_S n_e^2 dh \quad (\mathrm{cm}^{-5}), \tag{2}$$

where n_e is the electron number density, h is the LOS path length, and S is the region containing the physically interesting plasma (Kamio *et al.*, 2011). Under the assumption that the observed plasma is optically thin and in ionization equilibrium, the observed intensity of a single emission line along the LOS h is expressed as

$$I_\lambda = A_Z \int_S G(T, n_\mathrm{e}) n_\mathrm{e}^2 dh \quad (\mathrm{erg\ cm}^{-2}\ \mathrm{s}^{-1}\ \mathrm{sr}^{-1}), \tag{3}$$

where A_Z is the elemental abundance, and $G(T, n_\mathrm{e})$ is the contribution function containing the relevant atomic parameters. Equation (3) can then be used to simplify the EM definition to the form

$$\mathrm{EM} = \frac{F_\lambda}{A_Z G(T, n_\mathrm{e})} \quad (\mathrm{cm}^{-5}), \tag{4}$$

which is the standard definition for deriving EM loci curves. These curves, calculated per observed emission line, represent the EM under the assumption that the measured EM originates from an isothermal plasma at a given temperature. As such, their usefulness lies in their ability to reveal isothermal plasmas where all curves meet at one temperature (Kamio *et al.*, 2011).

Prior to measuring EM loci curves, contribution functions were calculated from the CHIANTI atomic database (Dere *et al.*, 1997, 2009) by using the ionization equilibriums of Arnaud and Raymond (1992), a typical quiet Sun electron density of 5×10^8 cm^{-3} (O'Dwyer *et al.*, 2010), and the photospheric abundances of Grevesse, Asplund, and Sauval (2007). EM loci curves were then calculated for each event and all observation times by using measurements of F_λ for each emission line in Table 2.

4. Results

Here we present the measurements for each event. As stated previously three events were identified: (a) an upper TR BP labeled EIS1a (lifetime, $\tau_\lambda \approx 1.5$ h), (b) a blinker labeled EIS1b ($\tau_\lambda \approx 3.2$ h), and (c) a CBP labeled EIS2 ($\tau_\lambda \approx 0.8$ h). Note that EIS1b occurred in the same ROI as EIS1a but appeared ≈ 4 h after EIS1a had disappeared. Table 2 presents the measurements of the three events. Below each event is discussed in turn.

Table 2. List of parameters derived for the three EIS events studied. "Obs.time" means initial time of observation. Angular brackets indicate time averages.

	Obs.time	τ_λ [h]	$\langle A \rangle$ [km^2]	$\langle P \rangle$ [erg s^{-1}]	$\langle \psi \rangle$ [%]	$\langle v \rangle$ [km s^{-1}]
EIS1a	11:13:11 UT	1.5	9.3×10^7	1.3×10^{22}	128	2.90
			2.4×10^8	1.2×10^{22}	29	12.4
EIS1b	16:49:18 UT	3.2	4.1×10^8	9.3×10^{21}	29	12.4
			1.1×10^9	5.3×10^{22}	11	47.1
EIS2	11:13:11 UT	0.8	1.2×10^7	1.7×10^{21}	209	17
			2.3×10^7	5.6×10^{22}	247	20.8

4.1. EIS1a — TR Bright Point

Figure 4 shows the temporal variation of the integrated line intensities F_λ (arbitrary units), LOS velocities v_λ (km s^{-1}), and emission enhancement ψ_λ (%) vs. time (s) in each of eight emission lines for the EIS1a event. The bulk of emission lines exhibited a significant increase in the integrated flux values F_λ during the first 45 min and had either returned to or dropped below their initial values 45 min later. EUV intensity enhancements ψ_λ were $\approx 40\%$ above the background for the TR lines but were negligible in the coronal lines. LOS velocities were

Line Intensity   Doppler Velocity   Line Enhancement
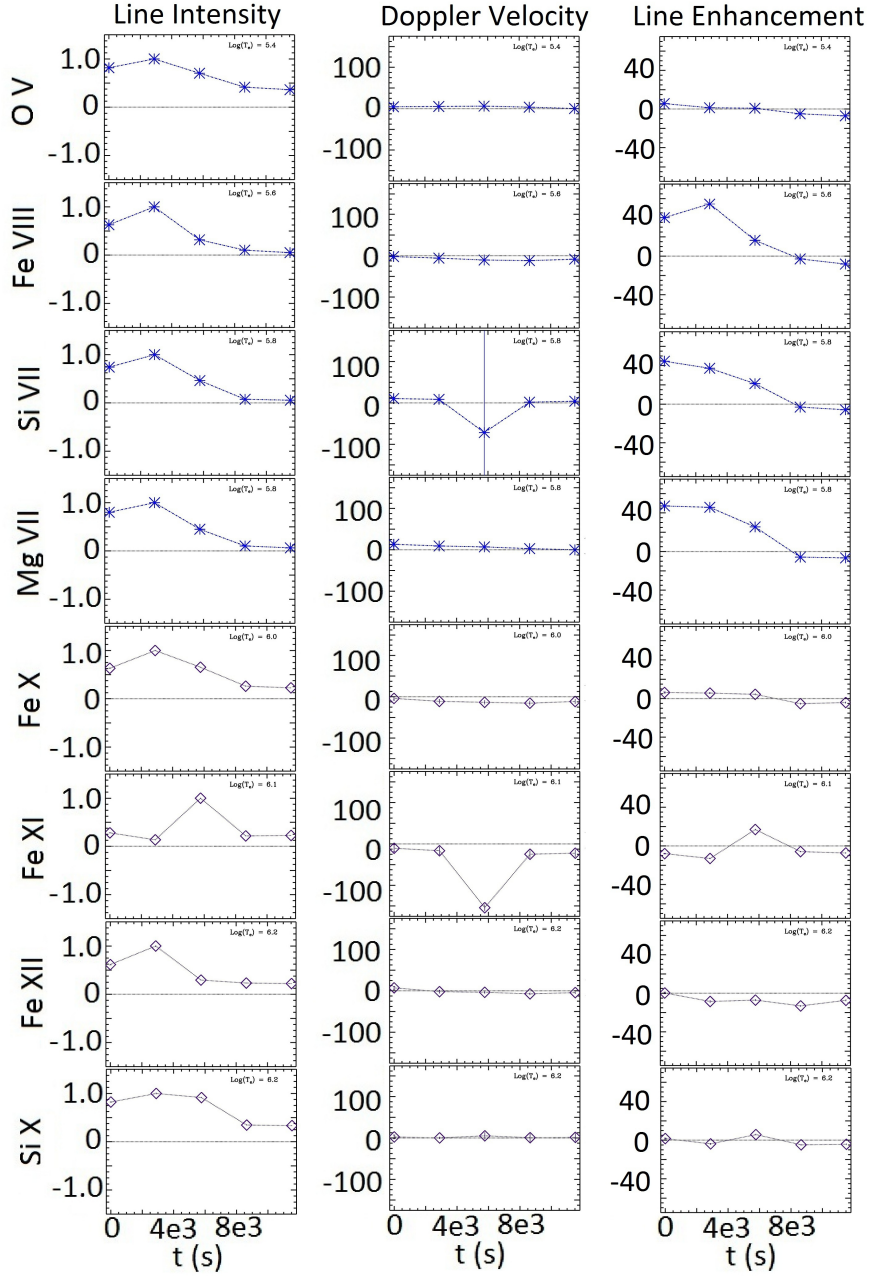
Figure 4. Integrated line fluxes F_λ (arbitrary units), LOS velocities v_λ (km s^{-1}), and emission enhancement ψ_λ (%) vs. time (s) in each of eight emission lines. The time is relative to 11:13:11 UT.

minimal in comparison to the surrounding background ($\lesssim \pm 20$ km s^{-1}) and were close to the resolution limit of velocities ($\approx \pm 5$ km s^{-1}).

In Figure 5 we have provided EUV intensity maps, LOS velocity maps, and MDI magnetic field contours at the time of peak emission, 12:01:18 UT. These images illustrate that the TR BP was thermally isolated within the TR as observed by previous authors. This is most notabe at $\log T = 5.8$ as observed in the emission of Fe VIII λ185.2, Si VII λ275.4, Mg VII λ278.4. At peak brightness, the size and luminosity of EIS1a in the TR was $\approx 9 \times 10^7$ km^2 and $\approx 1 \times 10^{22}$ erg s^{-1}, respectively. These values agree well with those reported for the TR BPs presented by Bruni (2006) as observed by the SUMER instrument in the emission of Ne VIII λ770.41 ($\log T = 5.8$). Likewise, the TR intensity enhancements are outside of the range previously reported for blinkers. Moreover, whereas blinkers have been mostly identified as EUV enhancements in the O V emission line (Harrison *et al.*, 1999), the TR BP EIS1a showed no significant O V emission.

The locations of event pixels identified by our boundary extraction function, which were used in our measurement of the characteristic LOS velocity of the event, are shown as contours on the Fe VIII λ185.2 intensity and velocity maps in Figure 5. Although significant plasma flows were observed in the vicinity of EIS1a at the time of peak brightness, the pixels spatially coincident with EIS1a do not show a strong Doppler signal. The values observed are $\lesssim \pm 20$ km s^{-1}, which is consistent with Doppler flows reported for quiet region CBPs (Madjarska *et al.*, 2003; Tian *et al.*, 2008; Pérez-Suárez *et al.*, 2008).

Co-spatial magnetic field data shows an interacting bipolar pair separated by ≈ 25 Mm, as illustrated on the Mg VII intensity map as green and blue contours. Until its complete cancellation at 12:49:19 UT, the separation distance of the flux pair was increasing at a rate of $\approx 2 \times 10^{-2}$ Mm min^{-1}. In Figure 6 we present the temporal evolution of the positive and negative fluxes. At the event onset, 11:13:11 UT, the positive and negative fluxes were $\approx \pm 2 \times 10^{18}$ Mx. Emerging positive flux occurred prior to the event's peak luminosity in EUV. During this peak the pair's typical positive and negative flux was $\approx 4 \times 10^{18}$ Mx. From the EUV flux peak till the event ceased to exist the bipolar pair canceled completely at a rate of $\approx 6 \times 10^{18}$ Mx h^{-1} (Figure 6).

The flux of the bipole is consistent with those expected in the TR (Pevtsov *et al.*, 2003) and values reported for TR BPs (Bruni, 2006), while observed cancellation rates are typical of CBP phenomena (Lee *et al.*, 2011; Zhang *et al.*, 2012). As expected, for BPs (Lee *et al.*, 2011; Kankelborg, Walker, and Hoover, 1997; Longcope *et al.*, 2001), both magnetic flux emergence and cancellation are found to be directly related to fluctuations of and brightening in solar EUV images. The flux pair's spatial divergence and magnetic flux evolution are considered as direct evidence of magnetic reconnection then.

Under the observed conditions either or both of the following can occur: formation of a null point above the flux pair as they come into contact which produces impulsive reconnection events (Priest, Parnell, and Martin, 1994), or a 2D-like current sheet forms along the fan-separatrix that is responsible for the long-lived nature of these brightenings (Pariat, Antiochos, and DeVore, 2010). Given the absence of any spectral signature of a vertically orientated jet (Zhang *et al.*, 2012), we consider our results indicative of the latter scenario. The diverging flux elements observed in magnetograms ≈ 6 h prior to our EIS observation sequence suggest that the flux pair forced the current sheet to an

orientation that was highly angled from the normal to the solar surface, *i.e.*, more horizontally directed. This seems a likely explanation for the minimal coronal emission enhancements, given that such field geometries would lead to plasma motion with higher velocity components parallel to the solar surface (Heggland, De Pontieu, and Hansteen, 2009). Such a scenario could explain the minimal enhancements of intensity images at temperatures cooler than $\log T = 5.4$, given the direction in which the heated plasma is propelled.

The TR intensity images, which shows emission "smeared out" away from a bright central core, are also consistent with this scenario. It is in the direction of this smearing that TR LOS velocity showed enhanced downflow regions which in relation to our above proposed scenario would be indicative of cooling and falling plasma as it spread out from the bright core. Furthermore, the positive x side of the event (*i.e.*, opposite side to the smearing) is visually dim and maybe be suggestive of plasma evaporation (Heggland, De Pontieu, and Hansteen, 2009) as a result of the reconnection events.

EIS1a's EM loci analysis indicates isothermal plasma is located at $\log T = 5.8$, where the convergence of multiple curves is observed (Figure 7). This is consistent with its similar visual appearance in emission lines sharing this formation temperature (the top row of Figure 5). Higher TR EMs in comparison with coronal EMs suggest condensation (Craig and McClymont, 1986). Otherwise, the TR loci curve distribution is relatively broad (Figure 11). This is perhaps indicative of unresolved structuring (Brooks, Warren, and Ugarte-Urra, 2012). Considering the previous notion that TR BPs are a self-similar phenomena to CBPs, which have been observed to be composed of flaring loop systems (Habbal and Withbroe, 1981; Habbal, Withbroe, and Dowdy, 1990; Koutchmy *et al.*, 1997; Krucker *et al.*, 1997; Tian *et al.*, 2008), one would expect the presence of both bi-directional flows (Athay *et al.*, 1982; 1983; Athay, Gurman, and Henze, 1983; Gebbie *et al.*, 1981) and unresolved structure (Zhang *et al.*, 2012).

The cooling of coronal plasma as the source of bright EUV emission is eliminated by noting the observed upward flowing plasma, ≈ 15 km s^{-1}, at $\log T = 6.0 - 6.2$. Moreover, these temperatures converge about the isothermal location. A more likely interpretation is that the conversion of magnetic to thermal energy took place over a small temperature regime, somewhere around $\log T = 5.8 - 5.9$. This is consistent with the bi-directional velocity pattern observed in LOS velocity images from the Fe VIII emission line (Figure 5), as well as suggestions by Heggland, De Pontieu, and Hansteen (2009) that such characteristics can be used as probes for reconnection heights. When we compare our observation of very small LOS velocities to those typically expected in jets resulting from newly reconnected field lines (Pariat, Antiochos, and DeVore, 2010; Kamio *et al.*, 2011), this further supports our suggestion that the dominant component of the outflow velocities are likely parallel to the solar surface. Given the uncertainty in the formation temperature Fe VIII (Del Zanna, 2012), we only suggest the reconnection events are occurring at the upper TR temperature of Fe. The cooling of heated upper TR plasma explains both the presence of redshifts and similarly structured brightenings in emission lines with formation temperatures close to this range. Furthermore, these inferences are consistent with previous suggestions on the current sheet orientation as well as minimal coronal EUV emission enhancements.

4.2. EIS1b — Blinker

The temporal evolution of integrated flux F_λ, LOS velocity v_λ, and EUV emission enhancements ψ_λ of the EIS1b event are provided in Figure 8. Its flux evolution exhibits a distinctive complex light curve in $\approx 75\%$ of the emission lines, with a secondary event being triggered at the conclusion of the first. The intensities of this latter event are typically $\approx 50\%$ less than the first while disappearing at temperatures of $\log T = 6.0 - 6.3$. The events are similar in terms of their durations (≈ 1.75 h) and their heating and cooling timescales (≈ 45 min). The time delay between intensity peaks is $\approx 6 \times 10^3$ s. This period is consistent with with $\approx 8\%$ of blinkers observed by Harrison *et al.* (1999), while both non-complex and complex light curves have been attributed to this phenomena (Brković and Peter, 2004).

The evolution of the EUV emission enhancement ψ_λ was consistent with the changes in the integrated flux as a function of temperature for EIS1b, with the exception of the Mg VII line whose temporal evolution was smooth and singly peaked (Figure 8) and occurred simultaneously with the onset of the second event. No significant difference in the magnitudes of the successive ψ_λ peaks was observed for this line. During this event, the O V $\lambda192.9$ ($\log T = 5.4$) peak intensity enhancement was $\approx 69\%$ while in the emission of Fe X $\lambda184.30$ ($\log T = 6.0$) it was $\approx 19\%$. These results, as well as the resultant TR to corona enhancement gradient, are typical of what has been observed for blinkers (Harrison *et al.*, 2003).

LOS velocities were $\lesssim \pm 20$ km s^{-1} except for the O V emission line which was ≈ 25 km s^{-1} on average. As observed in Figure 8, the O V LOS velocity evolution correlates well with that of the radiative flux in that the increases in downward flowing plasma correlate with the occurrence of increases in the EUV emission. These TR flow speeds are consistent with those observed in correlation with both quiet and active region blinkers (Madjarska and Doyle, 2003; Bewsher *et al.*, 2003; Brooks *et al.*, 2004). At $\log T = 6.0$ and 6.1, this same correlation between LOS velocity and radiative flux is observed for upward flowing plasma. This is suggestive of an upper TR bi-directional jet (Heggland, De Pontieu, and Hansteen, 2009).

Figure 9 provides intensity and LOS velocity maps as a function of temperature for EIS1b at 17:37:18 UT, which corresponds to the peak emission time of the first event. Visual inspection reveals a distinctly different morphology and intensity enhancement in the different emission lines. EIS1b was significantly dimmer for emission lines with peak formation temperatures of $\log T = 5.8$. In the TR the event was $\approx 4 \times 10^8$ km^2 in size with a luminosity of $\approx 9 \times 10^{21}$ erg s^{-1}. In the coronal lines it was an order of magnitude larger in both its projected area and its luminosity. Considering only a single heating and cooling event, the total energy radiated was $\approx 5 \times 10^{25}$ erg. Though the event's average size was three times larger than a typical blinker's, the resultant energy is consistent with the thermal energy estimates predicted by Harrison *et al.* (1997a,b) and observed by Harrison *et al.* (1999).

Magnetograms co-spatial with EIS1b were dominated by fragmented flux. The evolution of the positive and negative flux is shown in Figure 10. The absolute

value of the negative flux is $< 3 \times 10^{17}$ Mx throughout the observational sequence and was approximately three times greater than the positive flux. The dominant single polarity is typical of blinkers (Harrison *et al.*, 1999; Bewsher, Parnell, and Harrison, 2002) while the magnetic field strength is consistent with values reported for quiet region blinkers by Bewsher *et al.* (2002). The first peak in EUV intensity correlates with emergence of both positive and negative flux of $\approx 1.4 \times 10^{17}$ Mx and 2.7×10^{17} Mx, respectively. For the secondary event, the peak emission correlates with magnetic cancellation occurring at rates of $\approx 4.3 \times 10^{15}$ Mx min^{-1} and 8.6×10^{15} Mx min^{-1} for positive and negative flux, respectively.

In relationship to their EUV brightness, both the emergence and cancellation events are equivalent. However, the emergence event correlates with significantly higher EUV flux rates at both TR and coronal heights. These results indicate there exists no correlation between peaks in EUV brightness and the strength/evolution of the underlying magnetic field. Moreover, they are consistent with the conclusions that blinkers are a direct result of density enhancements by reconnection events by previous authors (Bewsher *et al.*, 2002; Harrison *et al.*, 2003).

Our EM loci analysis of EIS1b indicates weak isothermal components at $\log T = 6.1$ for observation times corresponding to peaks in emission. The EM loci curves of the first peak are shown in Figure 11. The absence of convergence for the cooler TR loci curves, as compared to those of the corona, indicates only the hotter coronal plasma is isothermal. Broad and approximately constant TR EM distributions, most notably at $\log T = 5.8$, are an indication of unresolved structure (Brooks, Warren, and Ugarte-Urra, 2012), which is consistent with the visual structuring of the event in intensity images (Figure 9).

The lower TR emission measure, compared to that of the corona, has been related to chromospheric evaporation (Craig and McClymont, 1986; McClymont and Craig, 1987). Under this interpretation coronal blue shifts indicate the heights to which chromospheric plasma is being heated, while pervasive TR redshifts are explained as a result of the cooling and condensing of the heated coronal plasma. This interpretation is preferred over heating from a bi-directional jet, as stated earlier, given that the magnetic field analysis indicated only a casual relationship between reconnection and EUV flux increases. We recognize that blinkers do not typically consist of isothermal plasma, at least in the TR, based on the fact that they are related to density-enhancements (Harrison *et al.*, 2003). However, under our proposed scenario it seems likely that the TR brightenings are due to density enhancements being generated via plasma heated to coronal temperatures.

4.3. EIS2 — Coronal Bright Point

The temporal evolution of the integrated flux F_λ, LOS velocities v_λ, and EUV emission enhancements ψ_λ of the EIS2 event are provided in Figure 12. Decreases in radiative flux occurred independent of temperature over the entire range of temperatures probed by our observations, *i.e.*, from $\log T = 5.4$ to 6.2. This implies that our temporal sequence witnessed only the cooling phase of this event or that the cadence of our EIS observations was longer than the typical

heating timescale. Based on the evolution of the emission enhancements, which showed increases or remained constant during the event's evolution, we have settled on the latter interpretation. Further support of this interpretation is found by considering that the brightness increases occurred on a timescale of ≈ 45 min, which are consistent with the observed CBP brightness oscillation periods (Tian *et al.*, 2008). Also our observed coronal emission enhancements (≈ 2.5 times that of the background) agree well with those reported for quiet region CBPs (Zhang *et al.*, 2012).

As with other events studied here, EIS2 is associated with very small LOS velocities at the bulk of temperature regimes studied. The exceptions are in the emission of O v $\lambda192.90$ at $\log T = 5.4$ and in the emission of Si x $\lambda274.14$ at $\log T = 6.2$, where the plasma was falling at a rate of ≈ 50 km s^{-1}. TR plasma downflow speeds are within the ranges observed in microflares (Berkebile-Stoiser *et al.*, 2009), while coronal flows are consistent with Kamio *et al.*'s (2011) results for microflarring CBPs. It is noted that these flow speed peaks correlate in time with peaks in the intensity enhancements ψ_λ of the respective emission lines (Figure 12).

We have provided both intensity and LOS velocity images in Figure 13 for the time of EIS2's peak irradiance. The intensity maps are consistent with previous reports of multi-thermal emission across the TR and corona for CBPs (Kankelborg, Walker, and Hoover, 1997; Kwon *et al.*, 2012). EIS2's typical size was $\approx 1 - 2 \times 10^7$ km^2 in both the TR and corona. Its luminosity ranged from $\approx 10^{21}$ erg s^{-1} to 10^{22} erg s^{-1} for the TR and corona, respectively. These sizes and lumnosities are very similar to those previously reported for CBPs by other authors (Pevtsov *et al.*, 2003; Longcope *et al.*, 2001).

The LOS velocity results shown in Figure 12 are consistent with the visual nature observed in Figure 13. Inspection of LOS velocity maps in Figure 13 reveal a distinctive bi-directional jet for the Si x ($\log T \approx 6.2$) emission line. EIS2 occurred co-spatially with the downflow jet ($\lesssim 50$ km s^{-1}) whose upward motion reached speeds of $\gtrsim 50$ km s^{-1}. This is expected since dimming and brightenings are most typically associated with blue-shifted and red-shifted regions, respectively (Craig and McClymont, 1986; McClymont and Craig, 1987). These flow speeds are consistent with Kamio *et al.*'s (2011) study, but are direct evidence that diffuse coronal jets can occur in conjunction with quiet region CBPs.

At 11:13:11 UT EIS2 occurred co-spatial with a bipolar pair in magnetograms, separated by ≈ 12 Mm. The evolution of positive and negative fluxes is provided in Figure 14. During the 45 min time span in which the EUV event existed, the bipolar pair's flux remained relatively constant (Figure 14), while the separation distance decreased by $\approx 40\%$. The typical magnetic flux associated with the bipolar pair was $\approx 3 \times 10^{18}$ Mx. Ultimately, the EUV event disappeared in conjunction with the complete cancellation of the photospheric bipole. We found the typical flux cancellation rate, of both positive and negative flux, to be $\approx 1 \times 10^{18}$ Mx h^{-1}.

EIS2's magnetic flux cancellation rate is consistent with those reported by Lee *et al.* (2011), while its longer time scale indicates that the resultant brightness increases are not explained by slow mode waves trapped within the magnetic flux

tubes constituting the structure (Doyle *et al.*, 1998; Ugarte-Urra *et al.*, 2004). Based on similarities in magnetic field changes between our event and those reported by Lee *et al.* (2011) and Zhang *et al.* (2012), we suggest that magnetic reconnection initiated by the convergence of the bipolar pair was responsible for the brightening observed in the EUV data. Moreover, these reconnection events were recurrent given that the typical timescale for coronal reconnection is tens of minutes (Chen *et al.*, 1999). In this proposed scenario the solar surface motions form a current sheet and build up magnetic energy near a null point of the assumed small-scale loop system comprising the CBP (Zhang *et al.*, 2012). Thus, successive and impulsive reconnection events may be triggered at the current sheet site until the flux pair has canceled completely (Pariat, Antiochos, and DeVore, 2010).

Isothermal analysis of EIS2 as shown in Figure 15 indicated that the event consisted of isothermal plasma around $\log T = 5.9$ at 11:13:11 UT. The occurrence of EM loci curves reaching higher than this location are indicative of an additional isothermal component (Kamio *et al.*, 2011). In Figure 15 both the O v and Fe xii EM loci curves are distributed significantly higher than the remaining emission lines, while intensity images of these lines share a distinctly similar bright EUV structure (Figure 13). From these results we hypothesize that O v was ionized at temperatures more typical of the corona. Therefore, the additional isothermal component is likely at $\log T \approx 6.2$.

5. Discussion

We have presented observations of a TR BP, blinker, and CBP, each recorded on 22 January 2008 during the 11:13:11 UT to 23:12:40 UT time frame, from multiple EIS emission lines along with accompanying MDI LOS magnetic field data. Our work has presented the first measurements of Doppler signatures associated with TR BPs as well as the first analyses of their detailed physical characteristics in multiple emission lines. With these data we may now identify the similarities and differences between the TR BPs and the CBP and blinker.

Our three events share a common characteristic in terms of their EUV morphology; they are all spatially compact and unresolved brightenings with characteristic sizes of $\approx 10^7$ km^2 – 10^8 km^2 (Figures 5, 9, and 13). As well, the luminosities of each of the three events were consistent with the luminosity versus unsigned magnetic flux relation of Pevtsov *et al.* (2003). We do note, however, that the emission enhancements of the BPs were more than four times larger than for the blinker.

The photospheric magnetic signatures of the TR BP and the CBP events were distinctly different from that of the blinker. The TR BP occurred on the neutral line of an interacting magnetic bipolar pair, suggesting that magnetic reconnection involving the said pair was responsible for its generation. This suggestion is supported by the appearance of the TR BP in EUV when the bipolar pair emerged followed by the observation that the EUV from the TR BP became undetectable after the bipolar pair was completely canceled. This behavior suggests that the generation mechanism of the TR BP involved reconnection

between the newly emerged bipole and surrounding background field, given the observed decreases in both positive and negative magnetic flux over its lifetime (Figure 6). Moreover, it is this characteristic that leads us to rule out the idea that this event is a direct result of slow magnetic reconnection which occurs as new flux emerges. The resultant heating energy of $\approx 10^{25}$ erg is consistent with nanoflares that impulsively heat the plasma during nanoflare "storms". This result supports the idea that like CBPs, TR BPs can be considered flaring loop systems where individual strands or small bundles are being rapidly heated and cooled at differing rates. Unfortunately, we were unable to resolve the heating time scales of the individual events and thus cannot directly infer the rate at which magnetic energy is converted to thermal energy via individual reconnection events. Nonetheless, the self-similar generation of the TR BP and CBP are an indication that TR and coronal heating are not fundamentally different for bright point phenomena. Moreover, it provides further support that the cooler BPs are a manifestation of multi-scaled self-similarity occurring in the solar atmosphere.

The connection between quiet region microflares and CBPs has been established (Kamio *et al.*, 2011), but only those occurring in coronal hole regions have been linked with jets. Our spectral analysis of CBPs, mainly the bi-directional jet observed at $\log T \approx 6.2$, indicates that jets may also exist in quiet regions, too. Thereby, we have provided the first observational evidence of the association between CBPs and jets in the quiet Sun. However, the difference in the large scale magnetic configuration yields a fundamental difference in the coronal hole and quiet region jets. That is, the coronal hole jets eject material nearly normal to the solar surface. This is consistent with the coronal hole events occurring in regions where the large-scale field is open (Kamio *et al.*, 2011). Our quiet Sun events appear to eject material in a direction that is nearly parallel to the solar surface. In essence, the plasma heating, radiation generation, and plasma ejection processes may be similar for TR BPs and CBPs. However, it is the large scale field configuration that determines the fate of any ejected material and whether the material is accelerated away from the Sun thus contributing to the solar wind flux, or whether the material falls back to the solar surface. The latter events are similar to explosive events (Beckers, 1968).

The single polarity dominated magnetic fields above which the blinker occurred are consistent with the idea that these events are generated by slow magnetic reconnection with pre-existing fields. We also observed significant emergence and cancellation events of the dominate polarity field occurring prior to the appearance of the said event, which is expected under the previous description of blinkers. We speculate, based on spectral results which showed no significant mass upflows, that this reconnection likely took place in the corona given the strong downflows found therein. However, the increases in this speed within the TR ($T \approx 0.25$ MK) are puzzling and are better described by a scenario in which multiple atmospheric locations are experiencing the said reconnection. We do recognize that the secondary event is fit by the description where reconnection only took place at coronal heights.

In terms of the applicability of isothermal assumption, only the blinker was non-isothermal, consistent with ideas that density/filling factor enhancements

are responsible for their generation (Harrison *et al.*, 2003). This description is also supported by the spectral data, which indicate significant downward flowing plasma that temporally correlated with peaks in EUV flux. These flows are interpreted as mass transfer from the corona to cooler portions of the atmosphere. The decreasing plasma speeds with decreasing temperature lead us to hypothesize that coronal energy was transported downward possibly via magnetoacoustic waves. Once these waves encounter the steep density gradient from the corona to the TR they steepen into shocks thereby heating the surrounding plasma. It is recognized that for this suggestion to be plausible for both the first and the second blinker events, such shocks would be required to initiate reconnection in the TR and propel mass downwards.

The loci plots of the TR BP and CBP show that the latter event was more resolved based on the visual inspection of the resultant EM distribution widths. We hypothesize that the TR BP was heated impulsively from below based on its EM loci and the form of its light curve. Minimal evidence was found for the existence of unresolved structure for this event, which indicates that our temporal cadence was unable to resolve the heating time scale. The TR BP shared no energetic connection with the corona which gives support to our earlier suggestion that its origin is most likely attributed to in-situ heating. We discount this emission event as a direct result of cooling coronal material by noting the absence of significant mass-flows throughout the coronal temperatures. However, it is recognized that our slower temporal cadence could have resulted in missed peaks in coronal emission line intensity. For the CBP a significantly greater portion of the plasma at the isothermal component was radiating. However, at this time the two identified isothermal components are more likely attributed to this event being a microflarring CBP, which could also just as likely explain its more spatially resolved nature.

The deluge of solar observational data from near-constant monitoring of the Sun is driving the need for frameworks that can quickly and automatically produce classifications of observed sources. Recent development of modern machine learning techniques and high performance computing architectures have made possible the efficient execution of automated probabilistic multi-class classification of very large datasets in reasonable time frames (Debosscher *et al.*, 2007; Sarro *et al.*, 2009a, 2009b; Debosscher *et al.*, 2009; Richards *et al.*, 2011, 2012; Blomme *et al.*, 2011; Matijevič *et al.*, 2012; Morgan *et al.*, 2012; Long *et al.*, 2012). An essential step in the development of such a framework is processing a large set of events of known class to train the classifier. The work presented here has indicated that similar measurements made across multiple event classes, *i.e.*, TR BP, blinker, and CBP, hold class-predictive power. Thereby, our work can be used in conjunction with similar studies (Chae *et al.*, 2000; Harrison *et al.*, 2003; Madjarska and Doyle, 2003; Brković and Peter, 2004; Bewsher *et al.*, 2005; Madjarska, Doyle, and De Pontieu, 2009) to begin facilitating a pathway which ultimately works towards automated multi-class classification of compact transients occurring in all temperature regimes of the solar atmosphere. As noted previously, this will be a major challenge of solar physics in the coming years. Finally it is emphasized that, the resultant large number statistics on a diversity of example structures across many classes from such a framework will allow a

reliable understanding of the underlying physical processes of these events to be achieved.

6. Conclusions

An investigation of a TR BP, blinker, and CBP, observed using *Hinode*/EIS, was carried out in this paper. For the first time, we have presented results on Doppler signatures of TR BPs. Similarities shared and distinct observational differences between these three events were highlighted. The relationship each event shared with the evolution of the underlying magnetic field was also studied and discussed. We concluded that the TR BP and CBP were a manifestation of solar atmospheric multi-scaled self-similarity, and that the heating of TR and coronal plasma were not fundamentally different in the presence of these phenomena. A connection between quiet region CBPs and jets was established, with indications that the said jets occur at high look angles compared to the solar surface due to the large scale magnetic configuration of the quiet Sun.

Finally, our work has shown that similar measurements across multiple event classes hold class-distinguishing capabilities, and as such are a significant step towards automated multi-class classification of compact transients occurring throughout the solar atmosphere. Further investigations are required on such events as those analyzed herein to resolve their heating timescales and determine conclusively if the origin of their bright TR emission is coronal or direct evidence of in situ heating.

7. Acknowledgements

References

Abramenko, V., Yurchyshyn, V., Goode, P., Kilcik, A.: 2010, Statistical distribution of size and lifetime of bright points observed with the New Solar Telescope. *Astrophys. J. Lett.* **725**, L101−L105. doi:10.1088/2041-8205/725/1/L101.

Arnaud, M., Raymond, J.: 1992, Iron ionization and recombination rates and ionization equilibrium. *Astrophys. J.* **398**, 394−406. doi:10.1086/171864.

Athay, R.G., Gurman, J.B., Henze, W.: 1983, Fluid motions in the solar chromosphere-corona transition region. III - Active region flows from wide slit Dopplergrams. *Astrophys. J.* **269**, 706−714. doi:10.1086/161080.

Athay, R.G., Gurman, J.B., Shine, R.A., Henze, W.: 1982, Fluid motions the solar chromosphere-corona transition region. II Active region flows in C IV from narrow slit Dopplergrams. *Astrophys. J.* **261**, 684 – 699. doi:**10.1086/160379**.

Athay, R.G., Gurman, J.B., Henze, W., Shine, R.A.: 1983, Fluid motions in the solar chromosphere-corona transition region. I - Line widths and Doppler shifts for C IV. *Astrophys. J.* **265**, 519 – 529. doi:**10.1086/160695**.

Beckers, J.M.: 1968, Solar spicules (invited review paper). *Solar Phys.* **3**, 367 – 433. doi:**10.1007/BF00171614**.

Berkebile-Stoiser, S., Gömöry, P., Veronig, A.M., Rybák, J., Sütterlin, P.: 2009, Multi-wavelength fine structure and mass flows in solar microflares. *Astron. Astrophys.* **505**, 811 – 823. doi:**10.1051/0004-6361/200912100**.

Bewsher, D., Parnell, C.E., Harrison, R.A.: 2002, Transition region blinkers I. Quiet-Sun properties. *Solar Phys.* **206**, 21 – 43. doi:**10.1023/A:1014954629349**.

Bewsher, D., Parnell, C.E., Brown, D.S., Hood, A.W.: Magnetic structure of transition region blinkers. In: Sawaya-Lacoste, H. (ed.) *SOLMAG 2002. Proceedings of the Magnetic Coupling of the Solar Atmosphere Euroconference, ESASP-505*, 239 – 242.

Bewsher, D., Parnell, C.E., Pike, C.D., Harrison, R.A.: 2003, Dynamics of blinkers. *Solar Phys.* **215**, 217 – 237. doi:**10.1023/A:1025642612049**.

Bewsher, D., Innes, D.E., Parnell, C.E., Brown, D.S.: 2005, Comparison of blinkers and explosive events: A case study. *Astron. Astrophys.* **432**, 307 – 317. doi:**10.1051/0004-6361:20041171**.

Blomme, J., Sarro, L.M., O'Donovan, F.T., Debosscher, J., Brown, T., Lopez, M., Dubath, P., Rimoldini, L., Charbonneau, D., Dunham, E., Mandushev, G., Ciardi, D.R., De Ridder, J., Aerts, C.: 2011, Improved methodology for the automated classification of periodic variable stars. *Mon. Not. Roy. Astron. Soc.* **418**, 96 – 106. doi:**10.1111/j.1365-2966.2011.19466.x**.

Brković, A., Peter, H.: 2004, Statistical comparison of transition region blinkers and explosive events. *Astron. Astrophys.* **422**, 709 – 716. doi:**10.1051/0004-6361:20040479**.

Brković, A., Solanki, S.K., Rüedi, I.: 2001, Analysis of blinkers and EUV brightenings in the quiet Sun observed with CDS. *Astron. Astrophys.* **373**, 1056 – 1072. doi:**10.1051/0004-6361:20010652**.

Brooks, D.H., Warren, H.P., Ugarte-Urra, I.: 2012, Solar coronal loops resolved by Hinode and the Solar Dynamics Observatory. *Astrophys. J. Lett.* **755**, L33. doi:**10.1088/2041-8205/755/2/L33**.

Brooks, D.H., Kurokawa, H., Kamio, S., Fludra, A., Ishii, T.T., Kitai, R., Kozu, H., Ueno, S., Yoshimura, K.: 2004, Short-duration active region brightenings observed in the extreme ultraviolet and Hα by the Solar and Heliospheric Observatory Coronal Diagnostic Spectrometer and Hida Domeless Solar Telescope. *Astrophys. J.* **602**, 1051 – 1062. doi:**10.1086/381089**.

Bruni, D.: 2006, A comprehensive study of bright points in the sun's upper transition region. Master's thesis, The University of Alabama in Huntsville.

Chae, J., Wang, H., Goode, P.R., Fludra, A., Schühle, U.: 2000, Comparison of transient network brightenings and explosive events in the solar transition region. *Astrophys. J. Lett.* **528**, L119 – L122. doi:**10.1086/312434**.

Chen, P.F., Fang, C., Tang, Y.H., Ding, M.D.: 1999, Simulation of magnetic reconnection with heat conduction. *Astrophys. J.* **513**, 516 – 523. doi:**10.1086/306823**.

Craig, I.J.D., McClymont, A.N.: 1986, Quasi-steady mass flows in coronal loops. *Astrophys. J.* **307**, 367 – 380. doi:**10.1086/164423**.

Culhane, J.L., Harra, L.K., James, A.M., Al-Janabi, K., Bradley, L.J., Chaudry, R.A., Rees, K., Tandy, J.A., Thomas, P., Whillock, M.C.R., Winter, B., Doschek, G.A., Korendyke, C.M., Brown, C.M., Myers, S., Mariska, J., Seely, J., Lang, J., Kent, B.J., Shaughnessy, B.M., Young, P.R., Simnett, G.M., Castelli, C.M., Mahmoud, S., Mapson-Menard, H., Probyn, B.J., Thomas, R.J., Davila, J., Dere, K., Windt, D., Shea, J., Hagood, R., Moye, R., Hara, H., Watanabe, T., Matsuzaki, K., Kosugi, T., Hansteen, V., Wikstol, Ø.: 2007, The EUV Imaging Spectrometer for Hinode. *Solar Phys.* **243**, 19 – 61. doi:**10.1007/s01007-007-0293-1**.

Debosscher, J., Sarro, L.M., Aerts, C., Cuypers, J., Vandenbussche, B., Garrido, R., Solano, E.: 2007, Automated supervised classification of variable stars. I. Methodology. *Astron. Astrophys.* **475**, 1159 – 1183. doi:**10.1051/0004-6361:20077638**.

Debosscher, J., Sarro, L.M., López, M., Deleuil, M., Aerts, C., Auvergne, M., Baglin, A., Baudin, F., Chadid, M., Charpinet, S., Cuypers, J., De Ridder, J., Garrido, R., Hubert, A.M., Janot-Pacheco, E., Jorda, L., Kaiser, A., Kallinger, T., Kollath, Z., Maceroni, C.,

Mathias, P., Michel, E., Moutou, C., Neiner, C., Ollivier, M., Samadi, R., Solano, E., Surace, C., Vandenbussche, B., Weiss, W.W.: 2009, Automated supervised classification of variable stars in the CoRoT programme. Method and application to the first four exoplanet fields. *Astron. Astrophys.* **506**, 519–534. doi:10.1051/0004-6361/200911618.

Del Zanna, G.: 2012, In-flight calibration of the Hinode EIS. Preliminary results. *ArXiv e-prints.*

Delaboudinière, J.-P., Artzner, G.E., Brunaud, J., Gabriel, A.H., Hochedez, J.F., Millier, F., Song, X.Y., Au, B., Dere, K.P., Howard, R.A., Kreplin, R., Michels, D.J., Moses, J.D., Defise, J.M., Jamar, C., Rochus, P., Chauvineau, J.P., Marioge, J.P., Catura, R.C., Lemen, J.R., Shing, L., Stern, R.A., Gurman, J.B., Neupert, W.M., Maucherat, A., Clette, F., Cugnon, P., van Dessel, E.L.: 1995, EIT: Extreme-Ultraviolet Imaging Telescope for the SOHO Mission. *Solar Phys.* **162**, 291–312. doi:10.1007/BF00733432.

Dere, K.P., Landi, E., Mason, H.E., Monsignori Fossi, B.C., Young, P.R.: 1997, CHIANTI - An atomic database for emission lines. *Astron. Astrophys. Suppl.* **125**, 149–173. doi:10.1051/aas:1997368.

Dere, K.P., Landi, E., Young, P.R., Del Zanna, G., Landini, M., Mason, H.E.: 2009, CHIANTI - An atomic database for emission lines. IX. Ionization rates, recombination rates, ionization equilibria for the elements hydrogen through zinc and updated atomic data. *Astron. Astrophys.* **498**, 915–929. doi:10.1051/0004-6361/200911712.

Doschek, G.A., Landi, E., Warren, H.P., Harra, L.K.: 2010, Bright points and jets in polar coronal holes observed by the Extreme-Ultraviolet Imaging Spectrometer on Hinode. *Astrophys. J.* **710**, 1806–1824. doi:10.1088/0004-637X/710/2/1806.

Dowdy, J.F. Jr.: 1993, Observational evidence for hotter transition region loops within the supergranular network. *Astrophys. J.* **411**, 406–409. doi:10.1086/172842.

Doyle, J.G., Roussev, I.I., Madjarska, M.S.: 2004, New insight into the blinker phenomenon and the dynamics of the solar transition region. *Astron. Astrophys.* **418**, L9–L12. doi:10.1051/0004-6361:20040104.

Doyle, J.G., van den Oord, G.H.J., O'Shea, E., Banerjee, D.: 1998, Waves in the solar transition region. *Solar Phys.* **181**, 51–71. doi:10.1023/A:1005078018623..

Egamberdiev, S.A., Iakovkin, N.A.: 1983, The luminiscence of bright X-ray points on the sun. *Dokl. Akad. Nauk Uzbek. SSR* **7**, 31–32.

Gebbie, K.B., Hill, F., November, L.J., Gurman, J.B., Shine, R.A., Woodgate, B.E., Athay, R.G., Tandberg-Hanssen, E.A., Toomre, J., Simon, G.W.: 1981, Steady flows in the solar transition region observed with SMM. *Astrophys. J. Lett.* **251**, L115–L118. doi:10.1086/183705.

Golub, L., Krieger, A.S., Vaiana, G.S.: 1976, Observation of spatial and temporal variations in X-ray bright point emergence patterns. *Solar Phys.* **50**, 311–327. doi:10.1007/BF00155294.

Golub, L., Krieger, A.S., Silk, J.K., Timothy, A.F., Vaiana, G.S.: 1974, Solar X-ray bright points. *Astrophys. J. Lett.* **189**, L93–L97. doi:10.1086/181472.

Grevesse, N., Asplund, M., Sauval, A.J.: 2007, The solar chemical composition. *Space Sci. Rev.* **130**, 105–114. doi:10.1007/s11214-007-9173-7.

Habbal, S.R., Withbroe, G.L.: 1981, Spatial and temporal variations of EUV coronal bright points. *Solar Phys.* **69**, 77–97. doi:10.1007/BF00151257.

Habbal, S.R., Withbroe, G.L., Dowdy, J.F. Jr.: 1990, A comparison between bright points in a coronal hole and a quiet-sun region. *Astrophys. J.* **352**, 333–342. doi:10.1086/168540.

Harrison, R.A.: 1997, EUV Blinkers: The significance of variations in the extreme ultraviolet quiet Sun. *Solar Phys.* **175**, 467–485. doi:10.1023/A:1004964707047.

Harrison, R.A., Fludra, A., Sawyer, E.C., Culhane, J.L., Norman, K., Poland, A.I., Thompson, W.T., Kjeldseth-Moe, O., Aschenbach, B., Huber, M.C.E., Gabriel, A.H., Mason, H.E.: 1997, Extreme ultraviolet observations of the solar corona: First results from the coronal diagnostic spectrometer on SOHO. *Adv. Space Res.* **20**, 2239–2248. doi:10.1016/S0273-1177(97)01059-4.

Harrison, R.A., Lang, J., Brooks, D.H., Innes, D.E.: 1999, A study of extreme ultraviolet blinker activity. *Astron. Astrophys.* **351**, 1115–1132.

Harrison, R.A., Harra, L.K., Brković, A., Parnell, C.E.: 2003, A study of the unification of quiet-Sun transient-event phenomena. *Astron. Astrophys.* **409**, 755–764. doi:10.1051/0004-6361:20031072.

Heggland, L., De Pontieu, B., Hansteen, V.H.: 2009, Observational signatures of simulated reconnection events in the solar chromosphere and transition region. *Astrophys. J.* **702**, 1–18. doi:10.1088/0004-637X/702/1/1.

Kamio, S., Hara, H., Watanabe, T., Fredvik, T., Hansteen, V.H.: 2010, Modeling of EIS spectrum drift from instrumental temperatures. *Solar Phys.* **266**, 209 – 223. doi:10.1007/s11207-010-9603-7.

Kamio, S., Curdt, W., Teriaca, L., Innes, D.E.: 2011, Evolution of microflares associated with bright points in coronal holes and in quiet regions. *Astron. Astrophys.* **529**, A21. doi:10.1051/0004-6361/201015715.

Kankelborg, C.C., Walker, A.B.C. II, Hoover, R.B.: 1997, Observation and modeling of soft X-ray bright points. II. Determination of temperature and energy balance. *Astrophys. J.* **491**, 952 – 966. doi:10.1086/304976.

Kankelborg, C.C., Walker, A.B.C. II, Hoover, R.B., Barbee, T.W. Jr.: 1996, Observation and modeling of soft X-ray bright points. I. Initial results. *Astrophys. J.* **466**, 529. doi:10.1086/177529.

Koutchmy, S., Hara, H., Suematsu, Y., Reardon, K.: 1997, SXR Coronal flashes. *Astron. Astrophys.* **320**, L33 – L36.

Krieger, A.S., Vaiana, G.S., van Speybroeck, L.P.: 1971, The X-ray corona and the photospheric magnetic field. In: Howard, R. (ed.) *Solar Magnetic Fields*, *IAU Symp.* **43**, 397.

Krucker, S., Benz, A.O., Bastian, T.S., Acton, L.W.: 1997, X-Ray network flares of the quiet Sun. *Astrophys. J.* **488**, 499 – 505. doi:10.1086/304686.

Kwon, R.-Y., Chae, J., Davila, J.M., Zhang, J., Moon, Y.-J., Poomvises, W., Jones, S.I.: 2012, Three-dimensional structure and evolution of extreme-ultraviolet bright points observed by STEREO/SECCHI/EUVI. *Astrophys. J.* **757**, 167. doi:10.1088/0004-637X/757/2/167.

Lee, K.-S., Moon, Y.-J., Kim, S., Choe, G.S., Cho, K.-S., Imada, S.: 2011, Two types of extreme-ultraviolet brightenings in AR 10926 observed by Hinode/EIS. *Astrophys. J.* **736**, 15. doi:10.1088/0004-637X/736/1/15.

Long, J.P., Karoui, N.E., Rice, J.A., Richards, J.W., Bloom, J.S.: 2012, Optimizing automated classification of variable stars in new synoptic surveys. *Publ. Astron. Soc. Pac.* **124**, 280 – 295. doi:10.1086/664960.

Longcope, D.W.: 1998, A model for current sheets and reconnection in X-Ray bright points. *Astrophys. J.* **507**, 433 – 442. doi:10.1086/306319.

Longcope, D.W., Kankelborg, C.C.: 1999, Coronal heating by collision and cancellation of magnetic elements. *Astrophys. J.* **524**, 483 – 495. doi:10.1086/307792.

Longcope, D.W., Kankelborg, C.C., Nelson, J.L., Pevtsov, A.A.: 2001, Evidence of separator reconnection in a survey of X-ray bright points. *Astrophys. J.* **553**, 429 – 439. doi:10.1086/320667.

Madjarska, M.S., Doyle, J.G.: 2003, Simultaneous observations of solar transition region blinkers and explosive events by SUMER, CDS and BBSO. Are blinkers, explosive events and spicules the same phenomenon? *Astron. Astrophys.* **403**, 731 – 741. doi:10.1051/0004-6361:20030397.

Madjarska, M.S., Doyle, J.G., De Pontieu, B.: 2009, Explosive events associated with a surge. *Astrophys. J.* **701**, 253 – 259. doi:10.1088/0004-637X/701/1/253.

Madjarska, M.S., Doyle, J.G., Teriaca, L., Banerjee, D.: 2003, An EUV bright point as seen by SUMER, CDS, MDI and EIT on-board SoHO. *Astron. Astrophys.* **398**, 775 – 784. doi:10.1051/0004-6361:20021732.

Madjarska, M.S., Huang, Z., Doyle, J.G., Subramanian, S.: 2012, Coronal hole boundaries evolution at small scales. III. EIS and SUMER views. *Astron. Astrophys.* **545**, A67. doi:10.1051/0004-6361/201219516.

Mariska, J.T., Warren, H.P., Ugarte-Urra, I., Brooks, D.H., Williams, D.R., Hara, H.: 2007, Hinode EUV Imaging Spectrometer observations of solar active region dynamics. *Publ. Astron. Soc. Japan* **59**, S713 – S719.

Matijevič, G., Prša, A., Orosz, J.A., Welsh, W.F., Bloemen, S., Barclay, T.: 2012, Kepler eclipsing binary stars. III. Classification of Kepler eclipsing binary light curves with locally linear embedding. *Astron. J.* **143**, 123. doi:10.1088/0004-6256/143/5/123.

McClymont, A.N., Craig, I.J.D.: 1987, Fast downflows in the solar transition region explained. *Astrophys. J.* **312**, 402 – 411. doi:10.1086/164885.

McIntosh, S.W., Gurman, J.B.: 2005, Nine years of EUV bright points. *Solar Phys.* **228**, 285 – 299. doi:10.1007/s11207-005-4725-z.

Morgan, A.N., Long, J., Richards, J.W., Broderick, T., Butler, N.R., Bloom, J.S.: 2012, Rapid, machine-learned resource allocation: Application to high-redshift gamma-ray burst follow-up. *Astrophys. J.* **746**, 170. doi:10.1088/0004-637X/746/2/170.

O'Dwyer, B., Del Zanna, G., Mason, H.E., Weber, M.A., Tripathi, D.: 2010, SDO/AIA response to coronal hole, quiet Sun, active region, and flare plasma. *Astron. Astrophys.* **521**, A21. doi:**10.1051/0004-6361/201014872**.

Pariat, E., Antiochos, S.K., DeVore, C.R.: 2010, Three-dimensional modeling of quasi-homologous solar jets. *Astrophys. J.* **714**, 1762 – 1778. doi:**10.1088/0004-637X/714/2/1762**.

Parnell, C.E., Bewsher, D., Harrison, R.A. doi:**10.1023/A:1015094119974.**.

Pérez-Suárez, D., Maclean, R.C., Doyle, J.G., Madjarska, M.S.: 2008, The structure and dynamics of a bright point as seen with Hinode, SoHO and TRACE. *Astron. Astrophys.* **492**, 575 – 583. doi:**10.1051/0004-6361:200809507**.

Pevtsov, A.A., Fisher, G.H., Acton, L.W., Longcope, D.W., Johns-Krull, C.M., Kankelborg, C.C., Metcalf, T.R.: 2003, The relationship between X-ray radiance and magnetic flux. *Astrophys. J.* **598**, 1387 – 1391. doi:**10.1086/378944**.

Priest, E.R., Parnell, C.E., Martin, S.F.: 1994, A converging flux model of an X-ray bright point and an associated canceling magnetic feature. *Astrophys. J.* **427**, 459 – 474. doi:**10.1086/174157**.

Raouafi, N.-E., Georgoulis, M.K., Rust, D.M., Bernasconi, P.N.: 2010, Micro-sigmoids as progenitors of coronal jets: Is eruptive activity self-similarly multi-scaled? *Astrophys. J.* **718**, 981 – 987. doi:**10.1088/0004-637X/718/2/981**.

Richards, J.W., Starr, D.L., Butler, N.R., Bloom, J.S., Brewer, J.M., Crellin-Quick, A., Higgins, J., Kennedy, R., Rischard, M.: 2011, On machine-learned classification of variable stars with sparse and noisy time-series data. *Astrophys. J.* **733**, 10. doi:**10.1088/0004-637X/733/1/10**.

Richards, J.W., Starr, D.L., Brink, H., Miller, A.A., Bloom, J.S., Butler, N.R., James, J.B., Long, J.P., Rice, J.: 2012, Active learning to overcome sample selection bias: Application to photometric variable star classification. *Astrophys. J.* **744**, 192. doi:**10.1088/0004-637X/744/2/192**.

Romano, P., Berrilli, F., Criscuoli, S., Del Moro, D., Ermolli, I., Giorgi, F., Viticchié, B., Zuccarello, F.: 2012, A comparative analysis of photospheric bright points in an active region and in the quiet Sun. *Solar Phys.* **280**, 407 – 416. doi:**10.1007/s11207-012-9942-7**.

Sánchez Almeida, J., Bonet, J.A., Viticchié, B., Del Moro, D.: 2010, Magnetic bright points in the quiet Sun. *Astrophys. J. Lett.* **715**, L26 – L29. doi:**10.1088/2041-8205/715/1/L26**.

Sarro, L.M., Berihuete, A.: 2011, Statistical techniques for the detection and analysis of solar explosive events. *Astron. Astrophys.* **528**, A62. doi:**10.1051/0004-6361/201014894**.

Sarro, L.M., Debosscher, J., López, M., Aerts, C.: 2009a, Automated supervised classification of variable stars. II. Application to the OGLE database. *Astron. Astrophys.* **494**, 739 – 768. doi:**10.1051/0004-6361:200809918**.

Sarro, L.M., Debosscher, J., Aerts, C., López, M.: 2009b, Comparative clustering analysis of variable stars in the Hipparcos, OGLE Large Magellanic Cloud, and CoRoT exoplanet databases. *Astron. Astrophys.* **506**, 535 – 568. doi:**10.1051/0004-6361/200912009**.

Scherrer, P.H., Bogart, R.S., Bush, R.I., Hoeksema, J.T., Kosovichev, A.G., Schou, J., Rosenberg, W., Springer, L., Tarbell, T.D., Title, A., Wolfson, C.J., Zayer, I., MDI Engineering Team: 1995, The Solar Oscillations Investigation - Michelson Doppler Imager. *Solar Phys.* **162**, 129 – 188. doi:**10.1007/BF00733429**.

Shimizu, T., Katsukawa, Y., Matsuzaki, K., Ichimoto, K., Kano, R., Deluca, E.E., Lundquist, L.L., Weber, M., Tarbell, T.D., Shine, R.A., Sôma, M., Tsuneta, S., Sakao, T., Minesugi, K.: 2007, Hinode calibration for precise image co-alignment between SOT and XRT (2006 November-2007 April). *Publ. Astron. Soc. Japan* **59**, S845 – S852.

Strong, K.T., Harvey, K., Hirayama, T., Nitta, N., Shimizu, T., Tsuneta, S.: 1992, Observations of the variability of coronal bright points by the Soft X-ray Telescope on YOHKOH. *Publ. Astron. Soc. Japan* **44**, L161 – L166.

Subramanian, S., Madjarska, M.S., Doyle, J.G.: 2010, Coronal hole boundaries evolution at small scales. II. XRT view. Can small-scale outflows at CHBs be a source of the slow solar wind? *Astron. Astrophys.* **516**, A50. doi:**10.1051/0004-6361/200913624**.

Subramanian, S., Madjarska, M.S., Doyle, J.G., Bewsher, D.: 2012, What is the true nature of blinkers? *Astron. Astrophys.* **538**, A50. doi:**10.1051/0004-6361/201117877**.

Tian, H., Curdt, W., Marsch, E., He, J.: 2008, Cool and hot components of a coronal bright point. *Astrophys. J. Lett.* **681**, L121 – L124. doi:**10.1086/590410**.

Ugarte-Urra, I., Doyle, J.G., Nakariakov, V.M., Foley, C.R.: 2004, CDS wide slit time-series of EUV coronal bright points. *Astron. Astrophys.* **425**, 1083 – 1095. doi:**10.1051/0004-6361:20041069**.

Vlahos, L., Georgoulis, M.K.: 2004, On the self-similarity of unstable magnetic discontinuities in solar active regions. *Astrophys. J. Lett.* **603**, L61 – L64. doi:10.1086/383032.

Webb, D.F., Martin, S.F., Moses, D., Harvey, J.W.: 1993, The correspondence between X-ray bright points and evolving magnetic features in the quiet sun. *Solar Phys.* **144**, 15 – 35. doi:10.1007/BF00667979.

Wilhelm, K., Curdt, W., Marsch, E., Schühle, U., Lemaire, P., Gabriel, A., Vial, J.-C., Grewing, M., Huber, M.C.E., Jordan, S.D., Poland, A.I., Thomas, R.J., Kühne, M., Timothy, J.G., Hassler, D.M., Siegmund, O.H.W.: 1995, SUMER - Solar Ultraviolet Measurements of Emitted Radiation. *Solar Phys.* **162**, 189 – 231. doi:10.1007/BF00733430.

Young, C.A., Gallagher, P.T.: 2008, Multiscale edge detection in the corona. *Solar Phys.* **248**, 457 – 469. doi:10.1007/s11207-008-9177-9.

Young, P.R., Del Zanna, G., Mason, H.E., Doschek, G.A., Culhane, L., Hara, H.: 2007, Solar transition region features observed with Hinode/EIS. *Publ. Astron. Soc. Japan* **59**, S727 – S733.

Zarro, D.M.: 2005, *IDL Map Software for Analyzing Solar Images*, http://orpheus.nascom.nasa.gov/zarro/idl/maps.html.

Zhang, J., Kundu, M.R., White, S.M.: 2001, Spatial distribution and temporal evolution of coronal bright points. *Solar Phys.* **198**, 347 – 365. doi:10.1023/A:1005222616375.

Zhang, Q.M., Chen, P.F., Guo, Y., Fang, C., Ding, M.D.: 2012, Two types of magnetic reconnection in coronal bright points and the corresponding magnetic configuration. *Astrophys. J.* **746**, 19. doi:10.1088/0004-637X/746/1/19.
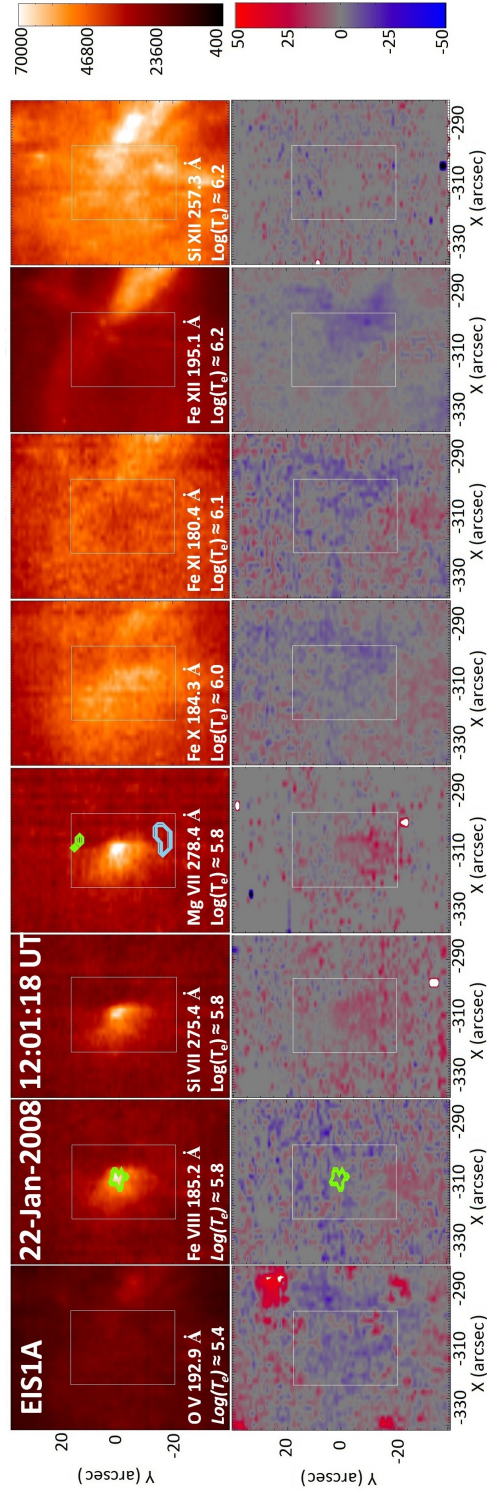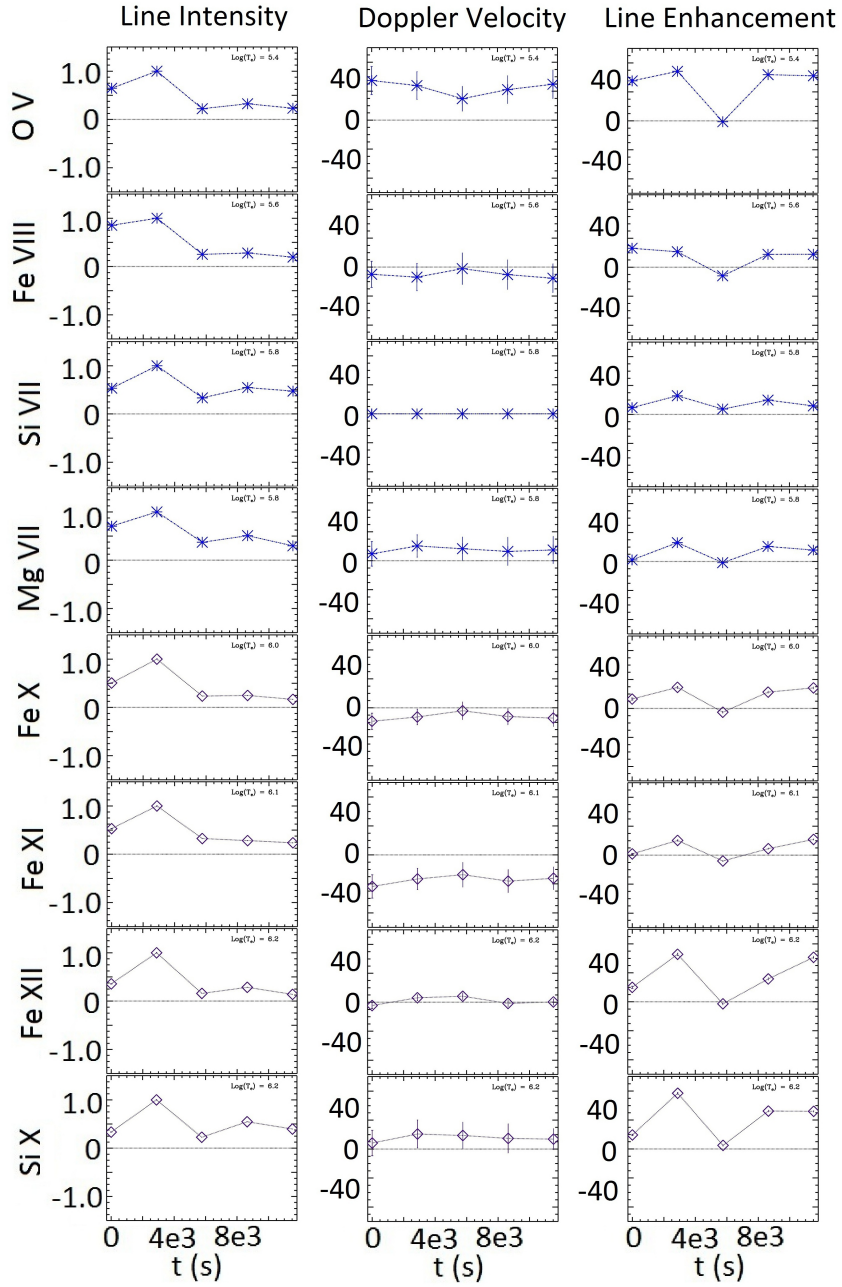
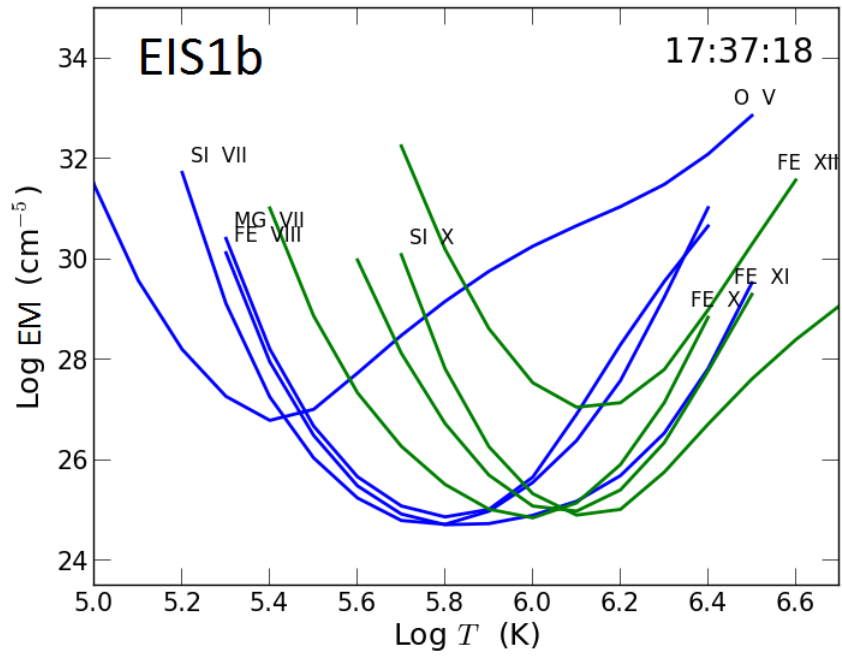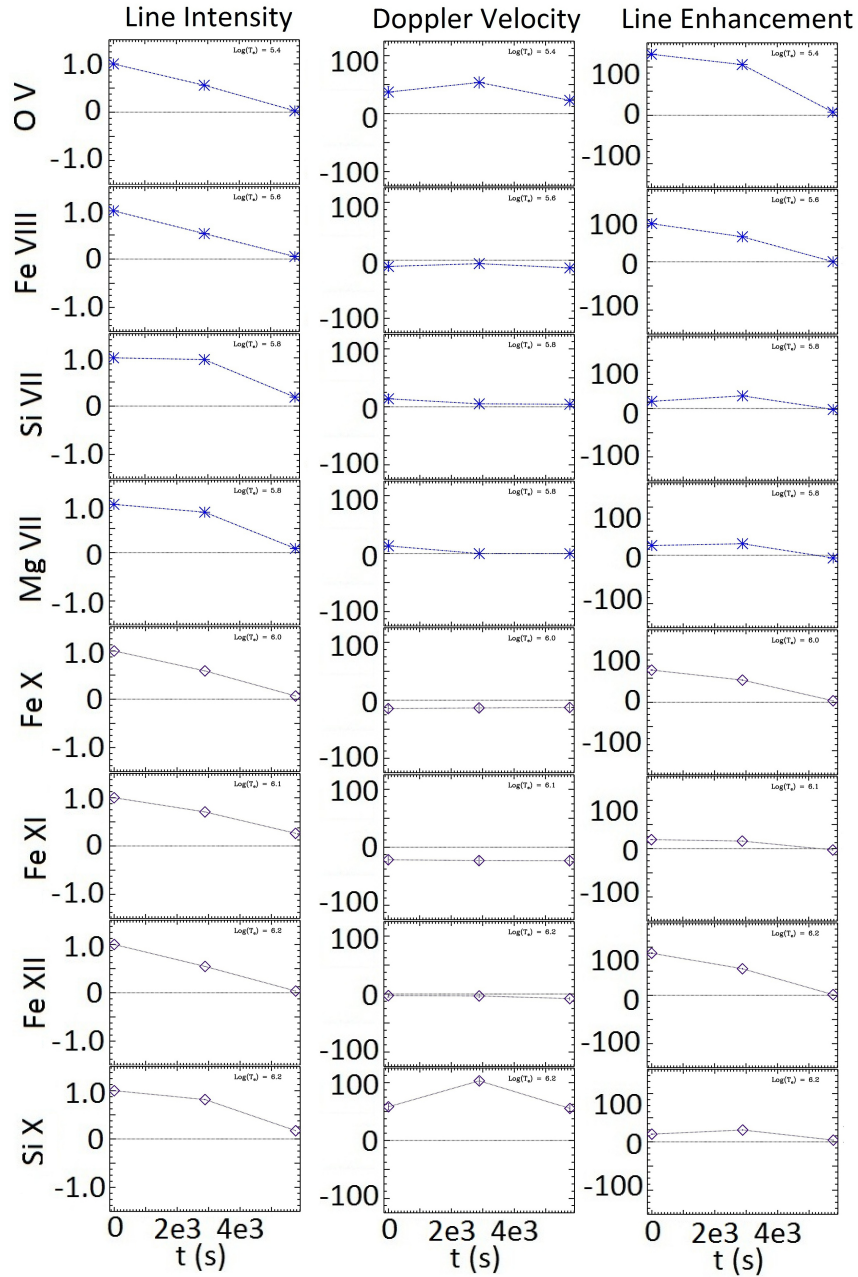**Figure 5.** Intensity and LOS velocity maps for EIS1a at the peak emission time, 12:01:18 UT. The squares indicate the areas selected for its analyses. Green contours on the Fe VIII intensity map denote the event pixels determined from our boundary extraction function. Green and blue contours on the Mg VII intensity image denote the locations of the positive and negative magnetic field patches.
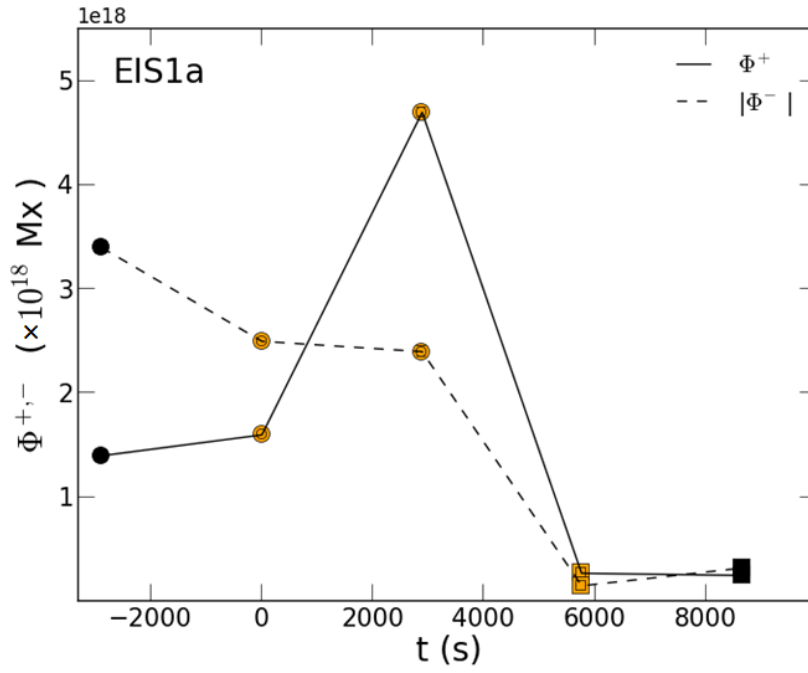
Figure 6. Positive (solid) and negative (dashed) magnetic fluxes ($\times 10^{18}$ Mx) as a function of time (s) for EIS1a. Square and circle symbols denote observations where the magnetic field configuration was fragmented and bipolar respectively, while orange marks observation times where the EUV event existed, $\approx 0 - 6 \times 10^3$ s. The time is relative to 11:13:11 UT.
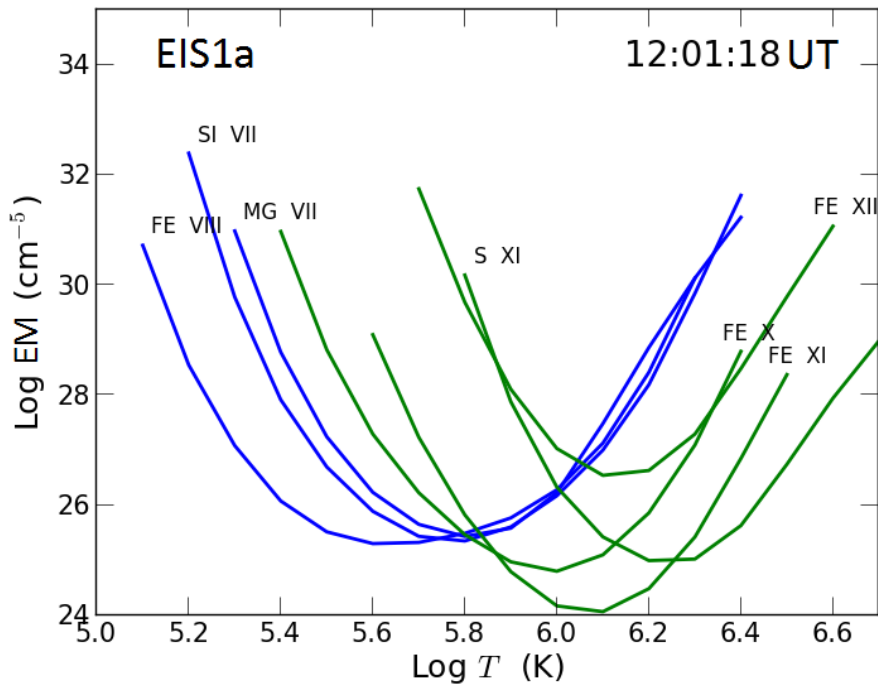
Figure 7. EM loci curves (blue and green represent TR and coronal emission lines, respectively) as a function of temperature for EIS1a at the time of peak enhancement (12:01:18 UT), showing a distinctive isothermal component around $\log(T) \approx 5.8$.

Figure 8. F_λ (arbitrary units), LOS velocity (km s^{-1}), and emission enhancement (%) vs. time (s) in columns from left to right, respectively, associated with EIS1b which existed over the 0 s $- 1 \times 10^4$ s temporal domain. It is noted the time is relative to 16:01:19 UT.
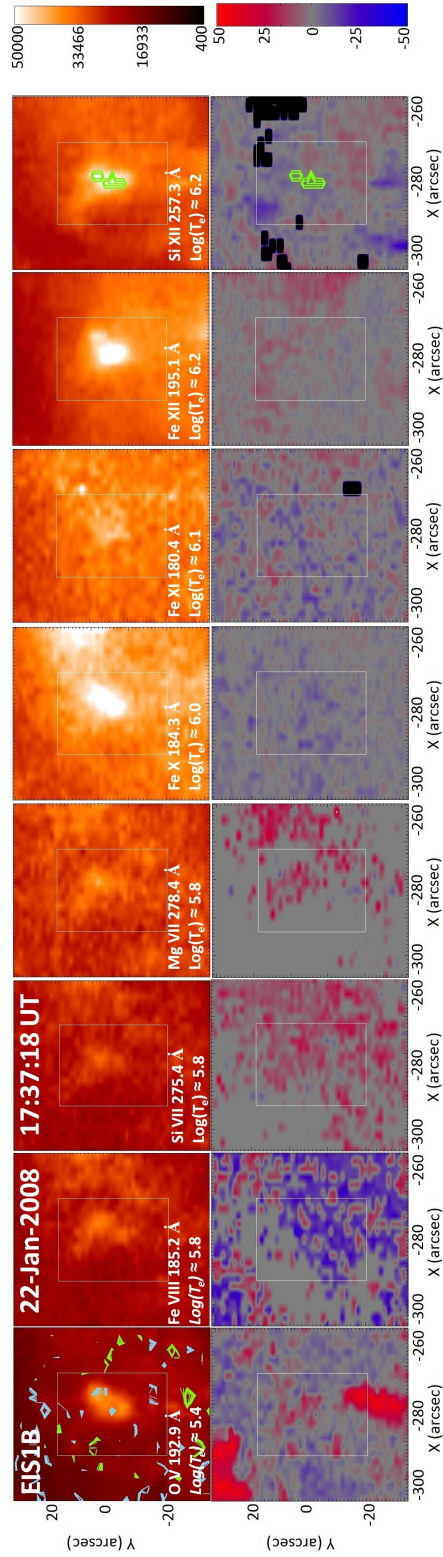
Figure 9. Intensity and LOS velocity maps for EIS1b at the peak emission time, 17:37:18 UT. The squares indicate the areas selected for its analysis. Green contours on the Si X intensity map denote the temperature regime in which they were defined and the spatial location identified as the event pixels. On the O VII intensity image green and blue contours represent positive and negative LOS magnetic field plotted at levels of $\pm 8 - 15$ G.
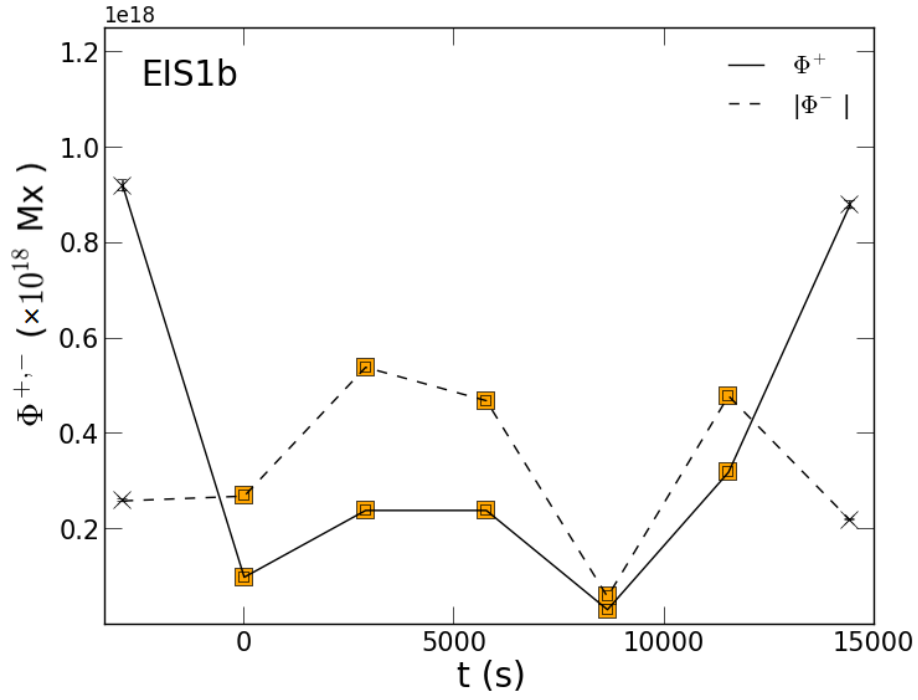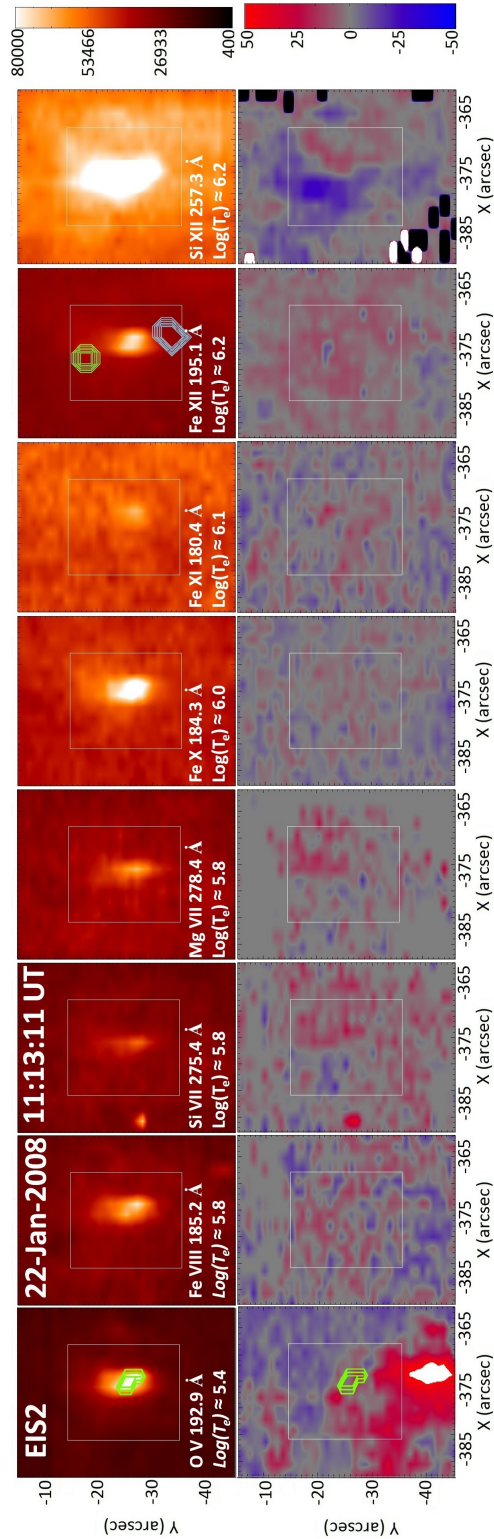
Figure 10. Positive (solid) and negative (dashed) magnetic fluxes ($\times 10^{18}$ Mx) as a function of time (s) for EIS1b. *Square* and *X* symbols denote observations where the magnetic field configuration was fragmented and unipolar respectively, while orange marks observation times where the EUV event existed, $\approx 0 - 1.1 \times 10^4$ s. The time is relative to 16:01:19 UT.
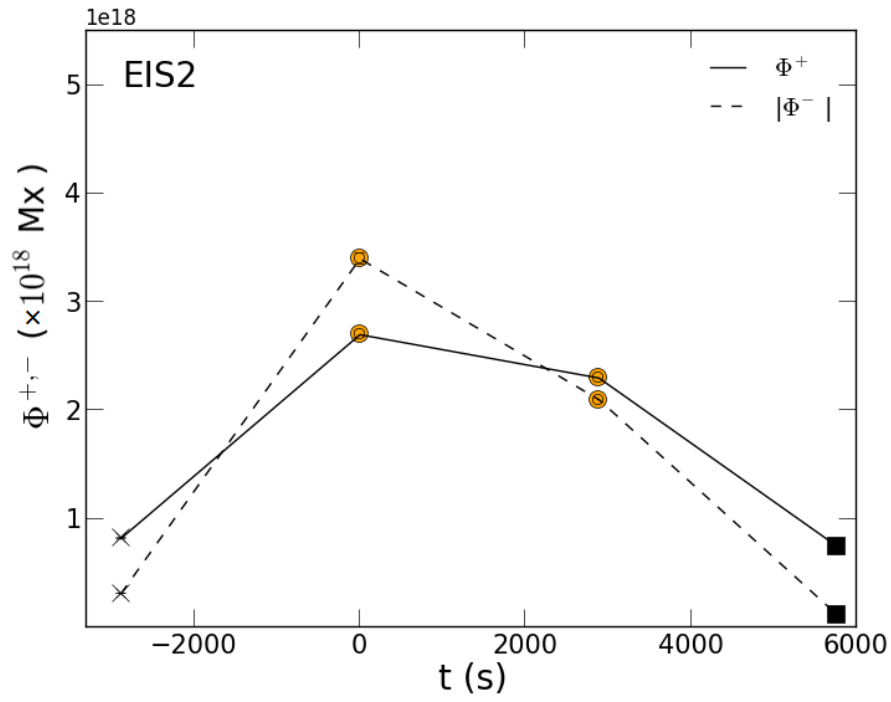
Figure 11. EM loci curves (blue and green represent TR and coronal emission lines, respectively) as a function of temperature for EIS1b at 12:01:18 UT, showing a mildly isothermal component around $\log(T) \approx 6.1$.

Figure 12. F_λ (arbitrary units), LOS velocities (km s^{-1}), and emission enhancement (%) vs. time (s) for EIS2 in columns from left to right, respectively. The times quoted are relative to 11:13:11 UT.

Figure 13. Intensity and LOS velocity maps for EIS2 at the peak emission time, 11:13:11 UT. The squares indicate the areas selected for its analysis. Green contours on the O V intensity map denote the temperature regime in which they were defined and the spatial location identified as the event pixels. On the Fe XII intensity image green and blue contours denote the locations of the positive and negative magnetic patches.

Figure 14. Positive (solid) and negative (dashed) magnetic fluxes ($\times 10^{18}$ Mx) as a function of time (s) for EIS2. Square, circle, and cross symbols denote observations where the magnetic field configuration was fragmented bipolar, and unipolar respectively, while orange marks observation times where the EUV event existed, $\approx 0 - 2.5 \times 10^3$ s.
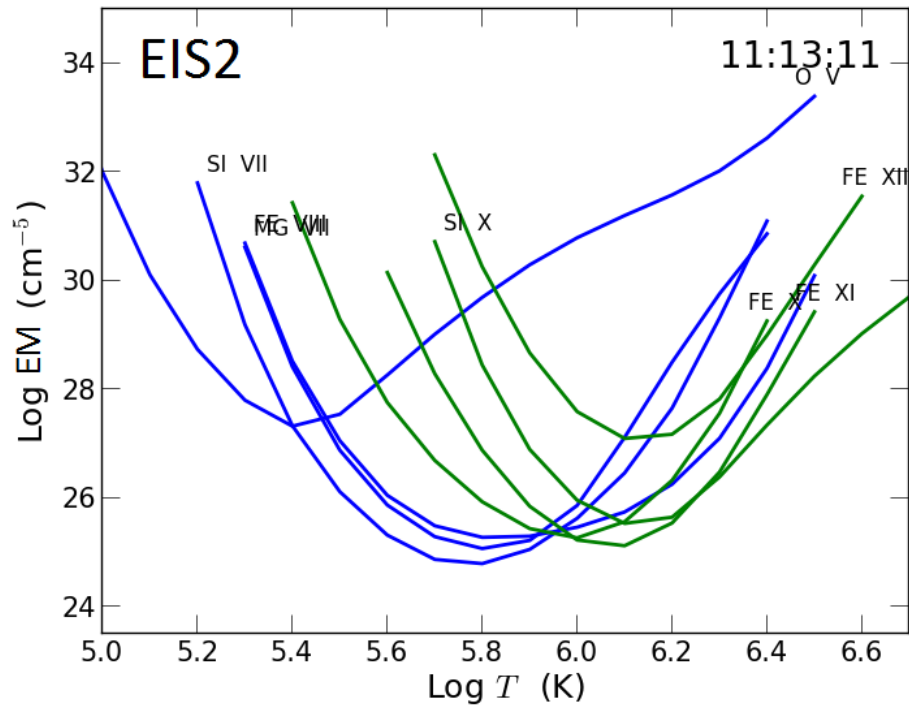
Figure 15. EM loci curves (blue and green represent TR and coronal emission lines, respectively) as a function of temperature for EIS2 at 12:01:18 UT showing a distinctive isothermal component around $\log{(T)} \approx 6.0$, and weaker secondary component around $\log{(T)} \approx 6.2$.